Coding transcriptome analyses reveal altered functions underlying immunotolerance of PEG-fused rat sciatic nerve allografts

Tyler A. Smith
University of Texas at Austin
Cameron L. Ghergherehchi
University of Texas at Austin
Haley O. Tucker
University of Texas at Austin
George Bittner (bittner@austin.utexas.edu)
University of Texas at Austin https://orcid.org/0000-0002-5610-6264

Research

Keywords: axotomy, Wallerian degeneration, polyethylene glycol (PEG), transplantation, allograft rejection, nerve repair, immune response, RNA sequencing, transcriptome

Posted Date: February 28th, 2020

DOI: https://doi.org/10.21203/rs.2.24814/v1

Version of Record: A version of this preprint was published on October 2nd, 2020. See the published version at https://doi.org/10.1186/s12974-020-01953-8.

Abstract

Background Current methods to repair ablation-type peripheral nerve injuries (PNIs) using peripheral nerve allografts (PNAs) often result in poor functional recovery due to immunological rejection as well as slow and inaccurate outgrowth of regenerating axonal sprouts. In contrast, ablation-type PNIs repaired by PNAs using a multistep protocol, in which one step uses the membrane fusogen polyethylene glycol (PEG), permanently restore sciatic-mediated behaviors within weeks. Axons and cells within the PNA remain viable, even though outbred host and donor tissues are neither immunosuppressed nor tissue matched. PEG-fused PNAs exhibit significantly reduced T cell and macrophage infiltration, apoptosis, and expression of major histocompatibility complex I/II. In this study, we analyzed the coding transcriptome of PEG-fused PNAs to examine possible mechanisms underlying immunosuppression. Methods Ablation-type sciatic PNIs in adult Sprague Dawley rats were repaired using PNAs and a PEG-fusion protocol combined with neurorrhaphy. Electrophysiological and behavioral tests confirmed successful PEG-fusion of PNAs. RNA sequencing analyzed differential expression profiles of protein-coding genes between PEG-fused PNAs and Negative Control PNAs (not treated with PEG) at 14d PO, along with Unoperated Control nerves. Sequencing results were validated by Quantitative Reverse Transcription PCR (RT-qPCR). Results PEG-fused PNAs display significant downregulation of many gene transcripts associated with innate and adaptive allorejection responses. Schwann cell-associated transcripts are often upregulated, and cellular processes such as extracellular matrix remodeling, cell and tissue development are particularly enriched. Transcripts encoding several potentially immunosuppressive proteins (e.g. Thrombospondins 1 and 2) are also upregulated in PEG-fused PNAs. Conclusions This study is the first to characterize the coding transcriptome of PEG-fused PNAs, and identifies possible links between alterations of the extracellular matrix and suppression of the allorejection response. The results establish a molecular-basis to begin to understand mechanisms underlying PEG-mediated immunosuppression.

Background

Traumatic peripheral nerve injuries (PNIs) affect approximately 1.6% of patients who have experienced upper- or lower-limb injury in the United States and Puerto Rico, resulting in life-altering neuronal deficits (1). Complete transection or ablation of a portion of a peripheral nerve results in immediate loss of reflex and voluntary behaviors and the Wallerian degeneration of all anucleated host axons distal to the injury site (and all anucleated axons in a peripheral nerve allograft (PNA)) within 1–5 days (2). Within hours, anucleated portions of axons release damage-associated molecular patterns (DAMPs) such as High Mobility Group Box 1 protein (HMGB1) and Adenosine Triphosphate (ATP), which are detected by Schwann cells and resident macrophages via Toll-Like Receptors (TLRs) (3, 4). This stimulation in combination with Wallerian degeneration of anucleate axons triggers Schwann cells to differentiate from a myelinating phenotype to a demyelinated phenotype (5). Demyelinated Schwann cells release cytokines and chemokines that recruit innate immune cells such as neutrophils and hematogenous macrophages to clear debris and assist the Schwann cells in facilitating regenerative outgrowths from surviving proximal axons that sometimes re-innervate distal targets. In mammals, this possible re-innervation is usually a very ineffective process that can take months to complete and often results in poor restoration of lost reflex and voluntary behaviors (2).

Simple transection PNIs are typically treated by re-apposing the cut ends with epineurial microsutures (neurorrhaphy), and ablation-type injuries are commonly repaired by neurorrhaphy in combination with peripheral nerve autografts taken from a different part of the patient's body (6). Although autografts are currently considered the "gold standard" to repair ablation-type PNIs, autografts produce loss of donor nerve function. Peripheral nerve allografts (PNAs) are an alternative to repair ablation-type PNIs. However, the immunogenicity of PNAs that contain living cells has severely limited their use for decades (7).

Within 7 days postoperatively, innate host immune cells responding to surgical injury recruit host T cells – the primary cells engaged in acute allorejection in the adaptive immune response (8, 9). Endogenous antigens, often presented by donor cells via Major Histocompatibility Complex Class I (MHCI) molecules (expressed on all nucleated cells) are recognized by host T cells expressing the CD8 co-stimulatory receptor, while exogenous antigens presented by MHCII molecules on either donor or host professional antigen presenting cells are recognized by host T cells expressing CD4 (10). Recognition of non-self antigens and/or MHC peptides often activate acute allorejection responses in host T cells to eliminate donor cells over a period of several weeks (7, 8). These allorejection responses of host T cells include proliferation and differentiation into effector phenotypes, cytokine and chemokine production to influence responses in nearby immune cells, killing of donor cells via perforins, granzymes, antibody-dependent cytotoxicity, and Fas receptor-mediated apoptosis. In PNAs, the primary targets of rejection are Schwann cells and endothelial cells, due to their abundance and their ability to express both MHCI and MHCII. Fibroblasts in PNAs may be also be targeted by T-cells (7).

Allorejection of PNAs is commonly avoided by using decellularized allografts, immunotolerant synthetic conduits, or systemic immunosuppressants such as FK506 (Tacrolimus) given to the host to suppress T cell activation by inhibiting Calcineurin signaling (11–14). However, decellularized PNAs and synthetic conduits lack endogenous Schwann cells and stromal cells to support axon regeneration, and immunosuppressant use can lead to opportunistic infections and liver damage. None of these techniques solve the long-existing problem of slow and ineffective restoration of nerve function after conventional neurorraphy.

PEG-fusion repair of singly transected sciatic PNIs in rats consists of neurorraphy to non-selectively join/fuse cut axonal ends by localized application of a well-defined sequence of four pharmaceutical agents in solution, including a high concentration (3.35kD) of the membrane fusogen polyethylene glycol (PEG) (15). PEG-fusion substantially improves morphological, functional, and behavioral recovery after single transection or ablation-type PNIs compared to current methods.

Animals treated with PEG-fusion repair of single transections re-establish morphological continuity and action potential conduction across the repair site within minutes, maintain axonal integrity and innervation of neuromuscular junctions,and prevent Wallerian degeneration for many myelinated axons. Successfully PEG-fused sciatic nerves restore sciatic-mediated voluntary behaviors to near unoperated levels within 42d post-operatively (PO) (16–18). Unexpectedly, these effects also are observed when ablation-type sciatic PNIs are repaired using PEG-fused PNAs that are neither tissue matched nor immune suppressed. Many donor axons within PEG-fused PNAs do not undergo Wallerian degeneration, strongly suggesting that the axons and Schwann cells within PEG-fused PNAs are not rejected.

We previously reported (19) that many innate and adaptive immune responses to PEG-fused PNAs were significantly reduced as assessed by transmission electron microscopy (TEM), immunohistochemistry (IHC), and quantitative reverse transcription PCR (RT-qPCR). Compared to Negative Control (NC) PNAs not treated with PEG at 14-21d PO, PEG-fused PNAs had significantly reduced T cell and macrophage infiltration, MHCI and MHCII expression, apoptosis, and expression of the pro-inflammatory cytokine interferon gamma (IFN-γ) and the T cell chemoattractant C-X-C motif chemokine ligand 11 (CXCL11). Although these data strongly suggested that an immunosuppressive environment was present within PEG-fused PNAs, the molecular activities associated with these effects were unknown.

We now describe molecular activities associated with non-rejection of PNAs as assessed by coding transcriptome profiles of PEG-fused PNAs at 14d PO—a time at which allorejection responses commonly manifest in NC PNAs (7, 20, 21). We report that 2,180 gene transcripts are differentially expressed when PEG-fused PNAs are compared to Negative Control PNAs. Consistent with our previous immunological analyses, RNA sequencing (RNAseq) revealed that an extensive array of transcripts encoding cytokines, chemokines, transcription factors, co-stimulatory molecules, and antigen presentation machinery necessary for innate and adaptive allorejection responses were significantly downregulated in PEG-fused PNAs. Many transcripts associated with Schwann cells in myelinating and demyelinated states were significantly upregulated, suggesting that Schwann cells associated with both intact and degenerated axons are not rejected.

We identified unanticipated links between alterations in the extracellular matrix and immunosuppression within PEG-fused PNAs. PEG-fused PNAs were particularly enriched in transcripts for extracellular matrix remodeling, cell adhesion, tissue development, fibroblast activity and collagen production. Many transcripts that encode immunosuppressive proteins such as Thrombospondins 1 and 2, CD24, and CD276 were also upregulated.

This transcriptomic study is the first to examine PEG-fused PNAs, and provides a crucial molecular foundation for understanding the mechanisms underlying PEG-mediated immunosuppression in PNAs, as well as other transplanted tissue types. Clinically, PEG-fused PNAs could potentially combine effective functional recovery with reduced rejection responses without decellularization or systemic immunosuppression.

Methods

Study design

The objective of this study was to use RNAseq to determine significant differences in the coding transcriptome profiles between PEG-fused PNAs, Negative Control PNAs (not treated with PEG), and Unoperated Control nerves. These differences suggest possible molecular mechanisms underlying PNA immunotolerance. Because acute rejection responses to allografts in rats typically reach their peak from 14-21d PO, PEG-fused sciatic nerve PNAs (n = 3 animals) and NC sciatic nerve PNAs (n = 3 animals) from outbred female Sprague Dawley rats rats (Envigo, RRID: RGD_737903) were excised and sampled at 14d PO (Additional File 1: Figure S1). Both treatment groups were compared to Unoperated Control sciatic nerves (n = 2 animals) as a baseline reference point for normal sciatic nerve function. DNase I-treated Total RNA was

extracted from each of the 8 samples and poly-A-enriched libraries were prepared and then sequenced on an Illumina next generation sequencing (NGS) platform. Initial analyses were conducted sequentially by FastQC, Tophat2, HTSeq-count, and DESeq2 software. Subsequently, analyses of gene ontology (GO) biological processes, protein families, pathways, and protein-protein interaction analyses were performed. Validation of RNAseq results for selected transcripts was performed via RT-qPCR.

Animals

All experimental procedures were approved by standards set forth by the Institutional Animal Care and Use Committee at the University of Texas at Austin. Female Sprague Dawley rats were housed 2–3/cage and maintained on a 12h:12 h reverse light:dark cycle with food and water given ad libitum. Surgical and behavioral procedures were performed in the active cycle. Animals used for behavioral assessments were handled and trained for behavioral testing (see below) for at least one week prior to surgery.

Brief description of PEG-fusion Protocol

The PEG-fusion protocol (see Fig. 1 of Ghergherehchi et al., 2019 (22) for details) consists of sequential administration of four pharmaceutical agents in solution directly applied to axonal cut ends and neurorrhaphy (microsutures through the epi- or perineurium): (1) Irrigation with 250 mM hypotonic Ca^{2+}-free saline for 1–2 min to increase axoplasmic volume, open cut axonal ends, and expel intracellular membrane-bound organelles. (2) Direct administration of the antioxidant methylene blue (MB) (1% in H_2O) for 1–2 min to the opened cut ends to prevent formation of new intracellular organelles that interfere with PEG-fusion of cut ends. (3) Neurorrhaphy to bring cut open ends of donor and host axons in very close apposition and to provide mechanical strength so that any PEG-fused axons within the nerve remained attached if the nerve is stretched. (4) Direct application of 50% w/w 3.35 kDa PEG in distilled water (i.e., 500 millimolal) for 1–2 min to remove bound cell water, thereby inducing any closely apposed, open, axonal membranes to fuse (repair/join). (5) Irrigation with isotonic Ca^{2+}-containing saline (290 mM) to induce vesicle formation to plug/repair/seal any axolemmal holes that may exist after PEG-induced annealing of the cytoplasm and axolemmas of open cut ends.

Surgical procedures

Outbred female Sprague Dawley Rats weighing 225–300 g were anesthetized with inhaled 4% isoflurane/oxygen mixture (Handlebar Anesthesia) at 1.5L/min and then maintained by a 1.5–2% mixture at 1L/min. PEG-fusion or NC Surgeries were performed on the lateral side of the left hindlimb. The right hindlimb served as an Intact Control.

A 2-3.5 cm incision was made through the skin and the left biceps femoris muscle to expose the sciatic nerve. Connective tissue around the sciatic nerve was trimmed with microscissors. Complete sciatic nerve transections were made in calcium-containing isotonic extracellular fluid and/or sterile isotonic Lactated Ringers (Dechra) by fine dissection scissors to completely sever all axons as well as their endo-, peri-, and epineural sheaths. A 6–8 mm segment was ablated in mid-thigh, leaving an 8–10 mm gap between cut axonal ends in the proximal and distal stumps of the host nerve. Because intact nerves were under tension, an ablation produces a gap that was several mm longer than the removed segment. For PNAs, a donor PNA that

matched the diameter of the host PNA was obtained from the left or right sciatic nerve of another wild type Sprague Dawley rat that was neither tissue matched nor immune-suppressed in donor or host. Donor PNAs were 1–3 mm longer than the gap created by the ablated segment of the host nerve and stored in calcium-free, hypotonic saline (Plasmalyte A (Baxter)) at 2°C for 30 min to 6hr before use. Identical procedures for neurorrhaphy and PEG fusion were performed for the proximal and distal ends of all PNA co-optation sites.

For all PEG-fused and NC groups, the PNAs and host sciatic nerves were washed with hypotonic Plasmalyte A and 1% methylene blue (MB) (Acros Organics). All axonal ends were carefully trimmed to provide smooth cut ends whose flat planes can be very closely apposed with at least four 10 − 0 microsutures through the epineurium. Nerves that were to be PEG-fused received a sterile hypotonic solution of 50% w/w 3.35 kDa PEG (Sigma Aldrich) in distilled water directly applied for 1–2 min to the lesion sites to non-specifically repair/fuse closely apposed cut axonal ends. After neurorrhaphy, lesion sites of PEG-fused and NC PNAs were washed several times with sterile isotonic Lactated Ringers containing calcium to repair any remaining axolemmal holes with calcium-induced vesicles or other membrane-bound structures. As previously described (16–19, 22), Compound action potentials (CAPs) and/or compound muscle action potentials (CMAPs) were elicited before severing any nerves, and again after PEG-fusion of PNAs by stimulating proximal to all lesion sites to insure that the procedure was successful. CAPs and CMAPs were not elicitable after nerve repair in Negative Control PNAs. Muscle incisions were closed with 5 − 0 sutures and the skin was closed with wound clips. Animals recovered from surgery on heated pads and were returned to standard housing. Animals to be tested for behavioral recovery received a 5 mg/kg subcutaneous injection of carprofen (Putney, Inc.).

RNA extraction

After sacrificing the animals using potassium chloride under anesthesia, Unoperated Control nerve segments (n = 2), 14d PO PEG-fused PNAs (n = 3), and 14d PO NC Allografts (n = 3) were immediately excised, sliced into 0.5 mm pieces with a scalpel blade, and stored in RNAlater (Invitrogen) overnight at 4 °C to prevent RNA degradation. The tissue was then placed onto a petri dish with TRIzol (Ambion) and minced into smaller pieces with scissors. The minced tissue along with the TRIzol was then transferred to a dounce homogenizer and ground until the previously white tissue became nearly transparent. Chloroform was added to the solution, the solution was centrifuged, and the extracted aqueous layer was then combined with an equal volume of 100% ethanol before transferring it to a RNeasy Mini kit (Qiagen) spin column (including RNase-free DNase I digestion) for RNA extraction. Total RNA concentration and purity was initially quantified with a Nanodrop 1000 spectrophotometer (Thermo Scientific, RRID:SCR_016517), and the RNA integrity was determined via BioAnalyzer 2100 (Agilent Technologies, RRID:SCR_018043). All RNA used for library preparation and RT-qPCR had RNA Integrity Numbers (RIN) between 7.1 and 8.2.

RNAseq and bioinformatic analyses

Prior to library preparation, total RNA sample concentration was quantified once again with a Qubit fluorimeter (ThermoFisher). Library preparation, sequencing, and initial bioinformatics analyses (generating differential expression results) were performed at University of Texas MD Anderson Science Park (MDACC) in Smithville, TX. Libraries for each individual sample (8 total samples) were generated with 0.13-4 µg of total RNA per sample using a TruSeq Stranded mRNA Library Prep kit (Illumina), according to instructions specified by the kit manufacturer. Libraries were sequenced on a single lane of a HiSeq 3000 unit (Illumina,

RRID:SCR_016386) for at least 20 million 75 bp paired-end reads per sample. Quality control of raw reads was performed using FastQC (RRID:SCR_014583). Tophat2 was used for mapping and alignment of reads to the reference genome Rnor 6.0 for Rattus norvegicus. Mapping rates ranged from 93.2–95%, while alignment rates ranged from 84.1–89.4% (Additional File 2: Table S1).

Read counts were then generated with HTSeq-count (RRID:SCR_011867). The DESeq2 Bioconductor package (RRID:SCR_015687) was used to generate normalized counts (median of ratios normalization method) and perform differential expression analyses (23). Hierarchical clustering of normalized reads and heatmap generation was performed using the “pheatmap” R package (RRID:SCR_016418) on normalized read counts. Correlation matrices were created using the “pheatmap” R package combined with the “cormat” R function. Principle Component Analysis (PCA) of normalized read counts between samples was performed using the “ggfortify” R package. Volcano plots of differentially expressed genes (DEGs) were generated using Graphpad Prism 8 software (RRID:SCR_002798).

Our selection criteria for DEGs were transcripts that had $\log_2$ fold changes > 1 or <-1and adjusted p-values (padj) < 0.05. Visualized networks of GO annotations for biological processes were generated using BiNGO 3.0.4 combined with Cytoscape 3.7 software (RRID:SCR_005736; RRID:SCR_003032) (24, 25). KEGG (Kyoto Encyclopedia of Genes and Genomes) pathway annotations (https://www.genome.jp/kegg) (RRID:SCR_012773) (26), and InterPro protein family annotations (https://www.ebi.ac.uk/interpro) (RRID:SCR_006695) (27) for DEGs were generated using DAVID 6.8 (Database for Annotation, Visualization, and Integrated Discovery (https://david.ncifcrf.gov) (RRID:SCR_001881) (28). Protein-protein interaction networks for all DEGs were generated using the STRING protein database (https://string-db.org) (RRID:SCR_005223) (29) combined with Cytoscape 3.7 software. STRING networks were generated using the default confidence threshold of 0.4 (medium confidence).

Quantitative reverse transcription PCR (RT-qPCR)

For PEG-fused and NC PNA samples, at least 200 ng of RNA per sample was reverse transcribed into cDNA using a High-Capacity cDNA Reverse Transcription Kit (Applied Biosystems). For Unoperated Control nerves, which contained lower amounts of RNA, 40 ng of RNA per sample was used. Samples were run on a PTC-200 thermocycler (MJ Research) according to guidelines provided by the kit manufacturer. 1 ng of cDNA and 500 nM of each primer per 20 µl reaction was used for quantitative PCR. Primers were designed via the PrimerQuest tool by Integrated DNA Technologies (IDT) using complimentary mRNA transcript sequences derived from National Center for Biotechnology Information (NCBI) GenBank databases for Rattus norvegicus (www.ncbi.nlm.nih.gov/genbank) (Table 1). qPCR reactions were prepared using PowerUp SYBR Green Master Mix (Applied Biosystems) and run for 40 cycles in triplicate on a ViiA7 qPCR thermocycler (Applied Biosystems) in a 96-well plate according to guidelines provided by the kit manufacturer. Glyceraldehyde 3-phosphate dehydrogenase (GAPDH) was used as a reference gene to normalize the expression data from other transcripts. RNA transcript expression for each gene, displayed as fold changes over Unoperated Control nerves, was quantified using the ΔΔCt method of relative quantification (30).

Table 1
Primer sequences used for RT-qPCR

Gene transcript	Accession number	Forward primer (5’-3’)	Reverse primer (5’-3’)
Shh	NM_017221.1	CTGGATTCGACTGGGTCTACTA	GGAAGCAGCCGTCAGATTT
Spp1	NM_012881.2	CACCAAGGACCAACTACAA	TGCCAAACTCAGCCACTT
Sox8	NM_001106989.1	CCCATGGTGAAAGCATGAAAG	TGGGAAAGACCTGTGGTAATG
Fbln5	NM_019153.3	CCTACTCCAATCCCTACTCTACA	TACCCAAAGCGACAGACAAG
Cd24	NM_012752.3	CTTGCCCATTCTGGGATCTAAT	GTTCCCGGGTAGGTTTCTAAAG
Ngfr	NM_012610.2	TCTGGCCAAAGAAGAGGATTAC	CATCCTGTGTGTGAGAGAGAAG
Col8a1	NM_001107100.1	CTCTACAGCTGCTGGGAATAC	GTGGTATCTGAGGAGGGATTTG
Ctsd	NM_134334.2	CACATCCTTCGACATCCACTAC	TCCACCTTGATACCTCCTAAGT
Thbs1	NM_001013062.1	ACTGAGAGGATGACGACTATG	GTAGGACTGGGTGACTTGTTTC
Thbs2	NM_001169138.1	CCCAGAGGCAGTTTGAGATT	CATCCTCCAGGAAGTTGGTATG
Icam1	NM_012967.1	GTATCCATCCATCCCACAGAAG	CAGTTGTGTCCACTCGATAGTT
Ccr5	NM_053960.3	GCTAGGCAGAGGAGAATGTTAG	TGTCTCCTCCTCCCAGTAAA
Ccl5	NM_031116.3	CAGAGAAGAAGTGGGTTCAAGA	GAGCAAGCAATGACAGGAAAG
Irf1	NM_012591.1	CTCACCAAGAACCAGAGGAAAG	AGATAAGGTGTCAGGGCTAGAA
Gzmb	NM_138517.3	AACCAGGAGATGTGTGCTATG	CCTCTTGTAGTGTGTCTGAGTATTT
Faslg	NM_012908.1	GGTGCTAATGGAGGAGAAGAAG	TAAATGGTCAGCAACGGTAAGA
Il10	NM_012854.2	AGTGGAGCAGGTGAAGAATG	GAGTGTCACGTAGGCTTCTATG
Nos2	NM_012611.3	TGGAGCGAGTTGTGGATTG	CCTCTTGTCTTTGACCCAGTAG
Cxcl11	NM_182952.2	GTGCCCTGCAAACATTTCTAC	GTGGGAAGCCAGTGTGATTA
Ifng	NM_138880.2	CGAATCGCACCTGATCACTAA	TGGATCTGTGGGTTGTTCAC

Statistical analyses

For RNAseq, differential expression between treatment groups and statistical analyses were performed using DESeq2, which uses negative binomial generalized linear models and the Wald Chi-Squared Test. p-values were adjusted with Benjamini-Hochberg correction. Transcripts with adjusted p-values (padj) < 0.05 were considered to be statistically significant in each comparison between treatment groups. Statistical analyses of GO annotation enrichment via BiNGO was performed using the Hypergeometric test and Benjamini & Hochberg False Discovery Rate correction; threshold padj < 0.05. Statistical analyses of KEGG and InterPro annotation enrichment via DAVID was performed using the Fisher Exact test, which determines whether the

proportions of transcripts falling into each annotation category differs by group; threshold p-value < 0.05. Comparisons of log fold changes for selected transcripts between RNAseq and RT-qPCR were made in Graphpad Prism 8 software, using the means and standard errors for each transcript. Correlation analyses of these selected transcripts were performed in Graphpad Prism 8, using parametric Pearson correlation analysis and linear regression. No data points or animal subjects used in this study were omitted; any outliers are included in each analysis.

Results

T cell and macrophage-associated transcripts are downregulated and Schwann cell-associated transcripts are upregulated in PEG-fused PNAs

We previously demonstrated through morphological and IHC analyses that PEG-fused PNAs had significantly reduced T cell and macrophage infiltration, and that these tissues contained many intact large-diameter axons that were still myelinated by accompanying Schwann cells (19). However, we had not yet investigated these cell types within PEG-fused PNAs for transcriptional profiles that may underlie particular activation states or cell subtypes.

To better understand the overall variance in normalized read counts (Additional File 3: Fig. S2A) for all transcripts among treatment groups and among individual samples, we performed Pearson correlation analyses and Principle Component Analyses (PCA) (Additional File 3: Figs. S2B, S2C). PCA indicated that individual samples within each treatment group clustered together, had similar expression profiles with no strong outliers, and the treatment groups themselves were biologically distinct from one another (Additional File 3: Fig. S2B). Strong sample-to-sample correlations in expression profiles were found within treatment groups, with PEG and NC groups showing greater correlation with each other than with the Unoperated Control group (Additional File 3: Fig. S2C).

We examined the normalized read counts for transcripts commonly expressed or associated with either T cells, macrophages, or Schwann cells. We created heat maps for which a given column is a sample and a given row is a gene. Transcripts were grouped according to expression patterns across rows (red = high expression; blue = low expression). Transcripts with statistically significant differences in expression (padj < 0.05) compared between PEG and NC groups were marked with an asterisk.

As shown in Fig. 1A, most transcripts associated with T cells and/or macrophages were downregulated in PEG-fused PNAs compared to NC PNAs. Initially focusing on T cells, downregulated transcripts included T helper 1 (Th1)-associated proinflammatory cytokines Interleukin 2 (IL2), Interleukin 12B (IL12B), Interferon Gamma (IFNG) and cytotoxic effectors that induce apoptosis in target cells, including Perforin (PRF1) and Granzyme B (GZMB) (8, 31–33). Notably, the cytokines Interleukin 4 (IL4), produced by Th2 cells, Interleukin 17A (IL17A), produced by pro-inflammatory Th17 cells (34), as well as Interleukin 10 (IL10) and Transforming Growth Factor Beta 1 (TGFB1) produced by immunosuppressive regulatory T cells which express Forkhead Box P3 (FOXP3) (35) also were downregulated in PEG-fused PNAs compared to NC PNAs. The transcription of co-stimulatory receptors (CD3, CD8, CD4, CD28, CD40LG), co-inhibitory receptors such as Cytotoxic T-Lymphocyte Associated Protein 4 (CTLA4) and Programmed Cell Death 1 (PDCD1), and downstream

transcription factors that drive T cell activation such as GATA Binding Protein 3 (GATA3) (10, 36) were downregulated in PEG-fused PNAs relative to NC PNAs. Although each of these representative transcripts were downregulated in PEG-fused PNAs relative to NC PNAs, they were significantly upregulated in PEG-fused PNAS relative to Unoperated Control nerves (Additional File 4: Table S2).

Likewise, macrophage-associated profiles revealed significant downregulation of numerous inflammatory "M1" macrophage-associated transcripts, including 1) the pro-inflammatory cytokine Interleukin 1 Beta (IL1B); 2) and Nitric Oxide Synthase (NOS2) involved in the respiratory burst attack response; and 3) Toll-like Receptors 1, 4, and 9 (TLR1/4/9), which are critical for initiating innate immune responses to damage- or pathogen-associated molecules (37). On the other hand, two transcripts commonly associated with the anti-inflammatory "M2" macrophage state, Arginase 1 (ARG1) and Mannose Receptor C type I (MRC1, also known as CD206), were highly expressed in PEG-fused PNAs, although not to a statistically significant degree when compared to NCs. Each transcript contributes to tissue repair and remodeling functions. Interestingly, the expression of CD68, which encodes a lysosomal protein involved in phagocytosis (38), was upregulated in PEG-fused PNAs. This finding was unanticipated based on our previous IHC analyses because CD68 immunostaining in 14d PO PEG-fused PNAs was decreased significantly relative to NC PNAs (19). Similarly to T cell-associated transcripts, macrophage associated transcripts were significantly upregulated in PEG-fused PNAs relative to Unoperated Control nerves (Additional File 4: Table S2).

Lastly, the expression of genes associated with the myelinating Schwann cell phenotype, including SRY-box 10 (SOX10), Myelin Basic Protein (MBP), and Myelin-Associated Glycoprotein (MAG) (5), were most highly expressed in Unoperated Control nerves (Fig. 1B). PEG-fused PNAs displayed upregulation of numerous transcripts associated with the demyelinated repair Schwann cell phenotype, which is triggered upon response to axonal injury. Examples include the AP-1 transcription factor subunit JUN, SRY-box 2 (SOX2), Nerve Growth Factor Receptor (NGFR), and Glial Derived Neurotrophic Factor (GDNF). Several additional transcripts associated with both myelinating and demyelinated Schwann cell phenotypes were significantly upregulated as well in PEG-fused PNAs compared to NC PNAs (Figs. 1C-H).

In this study, we defined the criteria for a differentially expressed gene (DEG) as having a $\log_2$ fold change in expression of >1 or <-1 and an adjusted p-value (padj) < 0.05. Volcano plots were employed to visualize these threshold criteria as applied to all transcripts when comparing PEG vs NC, PEG vs Unop, and NC vs Unop (Figs. 1I-K). PEG vs NC comparisons (Fig. 1I) yielded 1,433 downregulated DEGs and 747 upregulated DEGs.

The top 5 downregulated transcripts (ranked by padj) involved in chemokine/cytokine signaling and antigen presentation in T cells and myeloid cells. These include C-X-C Motif Chemokine Receptor 5 (CCR5), Interferon Regulatory Factor 1 (IRF1), Transporter 1, ATP Binding Cassette Subfamily B Member (TAP1), and Interleukin 2 Receptor Alpha (IL2RA) (10). Nicotinamide Phosphoribosyltransferase (NAMPT), the rate-limiting component within the NAD synthesis pathway, and an essential factor in lymphocyte survival, also was significantly downregulated (39). The top 5 upregulated transcripts in the PEG group consisted of Fibulin 5 (FBLN5), an integrin-binding matricellular protein that is upregulated during tissue injury and involved in endothelial cell adhesion (40), Laeverin (LVRN), an amino peptidase usually found in trophoblasts (41), Neuronal Cell Adhesion Molecular (NRCAM), involved in directional signaling during axonal cone growth (42), and Secreted Phosphoprotein 1 (SPP1), a matricellular protein that regulates tissue remodeling and cytokine

production (43). Both PEG vs Unop and NC vs Unop comparisons (Figs. 1J, K) showed downregulation of cell metabolic regulators Aldo-Keto Reductase Family 1 Member B (AKR1B1) and Phosphoenolpyruvate Carboxykinase 1 (PCK1), as well as the collagen subunit Collagen Type IV Alpha 4 Chain (COL4A4).

The top 5 upregulated transcripts from the PEG vs Unop comparison included primarily cell cycle progression mediators such as Topoisomerase 2A (TOP2A), Centromere Protein F (CENPF), and Cycline Dependent Kinase 1 (CDK1) (44). The top 5 upregulated transcripts from the NC vs Unop comparison primarily were composed of cytokine response modulators, such as CCR5, LYN Proto-Oncogene, Src Family Tyrosine Kinase (LYN), and NFAT Activating Protein with ITAM Motif 1 (NFAM1) (37). A complete listing of all normalized read counts and DEGs for all treatment group comparisons can be found in (Additional File 4: Table S2).

PEG-fused PNAs are enriched in extracellular matrix remodeling, cell adhesion, and tissue development processes

In order to determine which categories of biological processes and cellular pathways were enriched in each treatment group, we created a hierarchically clustered heatmap of all DEGs from the PEG vs NC comparison (2,180 DEGs total) (Fig. 2A). We divided the heatmap into four distinct clusters, based on k-means clustering of expression patterns between each treatment group. From each cluster we were then able to identify DEGs that were most highly expressed in the PEG group (Cluster 1; 347 transcripts), highly expressed in both PEG and in Unop (Cluster 2; 200 transcripts), most highly expressed in Unop (Cluster 3; 349 transcripts), and most highly expressed in NC (Cluster 4; 1,284 transcripts) (Figs. 2A, B) (Additional File 5: Table S3). The transcript IDs were extracted from each cluster and entered into BiNGO. This allowed us to derive functional annotations for biological processes via GO. We then validated the differential expression of 20 selected transcripts represented in Clusters 1, 2, and 4 via RT-qPCR (total of 10 upregulated transcripts and 10 downregulated transcripts) (Fig. 2C). The $\log_2$ fold change measurements for each gene transcript assayed via RT-qPCR very closely approximated those derived via RNAsEq. This result was confirmed by correlation analyses for all 20 transcripts, which yielded an R^2 of 0.97, Pearson correlation coefficient r of 0.98, and $p < 0.0001$ (Fig. 2D).

Unexpectedly, Cluster 1 was highly enriched in GO biological processes such as “collagen fibril organization” (COL1A1, COL1A2, LOX, COL5A1), “homophilic cell adhesion” (PCDHGA7, PCDH9, PCDH20, CDHR1), and “tissue development” (NGFR, IGFBP5, ELN, TGFB1I1) (Fig. 3A). The majority of protocaderins associated with “homophilic cell adhesion” are involved in neuronal process guidance and adhesion (45). Of note, a number of processes associated with fibroblast proliferation and migration were also highly enriched (Additional File 6: Table S4).

Transcripts highly expressed in both PEG and Unop groups in Cluster 2 were included in GO annotations that involve cell differentiation, Wnt signaling, and cyclic AMP (cAMP) signaling such as “Wnt receptor signaling pathway, calcium modulating pathway” (FZD2, WNT11, WNT16), “nervous system development” (RTN4R, GDF11, ARNT2, EDN3), “neural crest cell migration” (SHH, EDN3, SEMA3C, NRTN), and “cAMP metabolic process” (PDE1C, PDE3A, ADCY8) (Fig. 3B).

The transcripts most highly expressed in Unoperated Control nerves (Cluster 3) were primarily enriched in lipid metabolism, myelination, and ion transport functions, such as “fatty acid metabolic process” (FADS3, ACSL1,

SCD, LEP), “ion transport” (KCNK5, CLIC5, GRIK3, SLC4A1), and “regulation of action potential” (NFASC, P2RX5, KCNIP1, P2RX3) (Fig. 3C).

As expected from our previous examination of immune response in allografts (Smith et al., 2020), the transcripts most highly expressed in the Cluster 4 were enriched in processes such as “inflammatory response” (GATA3, IL1B, C4A, NFKB1), “regulation of T cell proliferation” (IL2, ZAP70, CD28, IFNG), and “antigen processing and presentation” (RT1-A1, RT1-DB1, B2M, TAP2) (Fig. 3D). Several transcripts in Cluster 4 also were found to be associated with muscle tissue development. This was expected since a thin layer of tightly-adhered muscle tissue and connective tissue surrounding rejected NC PNAs is a common occurrence (7, 17). Before excising the PNA, this muscle layer could not be completely trimmed from the PNA without damaging the PNA. Tabular listings of all BiNGO annotations and their associated transcripts can be found in (Additional File 6: Table S4).

Collagens, cadherins, and metallopeptidases are overrepresented in PEG-fused PNAs

Next, we identified which types of proteins were most highly represented in the list of transcripts that associated with GO annotations using the InterPro database, which classifies proteins by families, domains, and other identifiable features. Upon entering the gene transcript ID’s associated with each GO annotation from each cluster into the InterPro database via DAVID, we found that the top overrepresented protein families encoded by Cluster 1 transcripts included fibrillar collagen, laminin G domains, cadherins, protocadherins, epidermal growth factor (EGF)-like domains, thrombospondin type 1 repeats, metallopeptidases, and integrin alpha chains (Fig. 4). Top Cluster 2 proteins included more EGF-like domains, biotinidases, pyridoxal phosphate-dependent transferases, intermediate filament proteins, and adrenergic receptors, among others. Top Cluster 3 proteins were comprised of ion transport domains, fatty acid desaturases, P2X purinoceptors, cadherins, and phosphodiesterases. Lastly, Cluster 4 consisted of immunoglobulin-like folds, major histocompatibility class I and II antigen recognition proteins, chemokine interleukin-8-like domains, chemokine receptors, and death-like domains. A full list of all InterPro annotations with associated transcripts can be found in (Additional File 6: Table S4).

Downregulation of allograft rejection pathway and differential expression of particular integrins

To better understand the relationship between the transcripts that are differentially expressed in the PEG vs NC comparison, we used DAVID to identify the most highly enriched KEGG pathways associated with each cluster (Additional File 6: Table S4). We then selected the most enriched KEGG pathway in Cluster 1 (“ECM-receptor interaction”) and the second-most enriched KEGG pathway for Cluster 4 (“Allograft rejection”), and mapped all 2,180 DEGs from the PEG vs NC comparison to the two pathway diagrams (Figs. 5A, B). The diagram for the most enriched KEGG pathway in Cluster 4 (“Cytokine-cytokine receptor interaction”) was too large to include as a figure.

We found that all DEGs that mapped to the “Allograft rejection” pathway were downregulated (Fig. 5A). These transcripts were involved in functions such as antigen presentation in both direct and indirect allorecognition

pathways, T cell and B cell receptor signaling, and donor cell killing. In the “ECM-receptor interaction” pathway, all of the mapped DEGs were upregulated with the exception of those that encoded alpha 4, alpha IIb, and beta 6 integrin subunits (Fig. 5B). These integrins are integral to T cell infiltration across the endothelium, platelet aggregation during wound healing, and fibronectin binding, respectively (46). Collagens, laminins, reelins, thrombospondins, and SPP1 were highly prominent among upregulated DEGs, as were alpha 7 and alpha V integrin subunits, which encode proteins that form interactions with basement membranes and a wide variety of other ligands.

PEG-fused PNAs upregulate factors commonly involved in immunosuppression

After functional annotation analyses, we identified several DEGs from Cluster 1 that could contribute to an immunosuppressive environment in PEG-fused PNAs, including CD24, Thrombospondin 1 (THBS1), Thrombospondin 2 (THBS2) and CD276.

CD24 is a glycophosphatidylinositol (GPI)-linked protein presented on the surface of many cells associated with the nervous system and immune system and contributes to a variety of functions (47). In the immune system, CD24 expressed in antigen presenting cells binds to the sialic acid binding lectin Siglec-10 on macrophages (48). Siglec-10 closely associates with the tyrosine phosphatases SHP-1 and SHP-2, which negatively regulate nuclear factor kappa B (NF-κB) signaling. Thus, interaction of Siglec-10 with CD24 results in suppression of TLR-mediated inflammatory signaling in response to tissue damage, as well as in phagocytic clearance. The immunosuppressive microenvironment of many tumors correlate with CD24 overexpression. CD24 overexpression in PEG-fused allografts may contribute to similar effects.

THBS1 and THBS2 are large homotrimeric extracellular matrix binding proteins transiently expressed in fibroblasts, Schwann cells, and endothelial cells. They support remodeling and assembly of the collagen matrix (among many other functions) following tissue damage and inflammation (49, 50). Both proteins are structurally similar, and their overexpression confers potent anti-inflammatory properties (51, 52). These include drastically reduced inflammation, T cell infiltration, production of IFN-γ, and differentiation of T cells into their effector phenotypes. The latter mechanism likely occurs through interaction with the CD47 antigen on the T cell surface. Binding of CD47 may interfere with antigen-mediated signaling in T cells and sensitize them to Fas-mediated apoptosis.

The type I transmembrane protein CD276/B7-H3 is an influential immune checkpoint that is a component of the B7/CD28 costimulatory activation pathway in T cells (53). CD276 is commonly expressed in fibroblasts and endothelial cells following induction in antigen presenting cells. Overexpression of CD276 is a common mechanism by which tumor cells evade the adaptive immune response in many forms of cancer. In T cells, a combination of B7-1/2 and CD28 co-stimulation with the peptide/MHC complex is required for full activation of Th1 responses (10). CD276 can bind to CD28 on T cell surfaces, and thus, inhibit T cell activation of Th1 responses and proliferation by acting as a co-inhibitory molecule to suppress the transcriptional activity of Nuclear Factor Kappa B (NF-kB), Nuclear factor of activated T-cells (NFAT), and AP-1. This suppression prolongs allograft survival (54).

To determine which other proteins encoded by DEGs from the PEG vs NC comparison interact with those encoded by CD24, THBS1, THBS2, and CD276, we created STRING protein-protein interaction networks (Figs. 6A-C). STRING displays networks that have known or predicted protein-protein interactions, based on experimental determination, computational prediction, and public text-mining. All transcripts associated with Clusters 1, 2, and 4 were used as input to generate the networks, along with their fold change values to indicate upregulation or downregulation of each transcript. Among upregulated transcripts, we found that CD24 associated with Sonic Hedgehog (SHH) and SOX2 (Fig. 6A). SOX2 encodes a transcription factor that in part promotes the demyelinating Schwann cell state, and also directly upregulates CD24 expression by binding to its promoter (55). CD24 associated with a number of Cluster 4 downregulated transcripts that are linked to immune responses, such as CD28, IL2, and CD3E. THBS1 and THBS2 were primarily associated with upregulated extracellular matrix transcripts, including collagens, integrins, and metalloproteases (Fig. 6B). Downregulated transcripts that associated with THBS1 and THBS2 were involved in coagulation and adhesion to endothelial cells such as Fibrinogen Gamma Chain (FGG), Intercellular Adhesion Molecular 1 (ICAM1), and Vascular Adhesion Molecule 1 (VCAM1). CD276 associated with a wide variety of downregulated immune response transcripts from Cluster 4, which includes chemokines, cytokines, costimulatory molecules, and adhesion molecules.

Discussion

Summary of findings

We previously reported that PEG-fused sciatic PNAs in rats maintained morphological and electrophysiological continuity, did not undergo Wallerian degeneration, maintained large-caliber myelinated axons that were not rejected, maintained highly innervated distal neuromuscular junctions, and had improved behavioral recovery for up to 42d PO (17). We also reported that PEG-fused PNAs had reduced innate and adaptive inflammatory responses in the form of significantly reduced T cell and macrophage infiltration, MHC I and II expression, apoptosis, and expression of IFN-γ and CXCL11 (19).

In the present study, we assessed PEG-fused PNAs using transcriptomic analyses. Differential gene expression, GO biological processes, KEGG pathways, and InterPro protein families were compared between PEG-fused PNAs and NC PNAs at 14d PO—a time when inflammatory and rejection responses are well underway in NC PNAs. We compared these data with similar data from Unoperated Control sciatic nerves.

Transcriptomic analyses in PEG-fused PNAs compared to NC PNAs revealed downregulation of many T cell and macrophage-associated transcripts and upregulation of many Schwann cell-associated transcripts in both myelinating and demyelinated states. Compared to Unoperated Control nerves, PEG-fused PNAs upregulated the same T cell, macrophage, and demyelinated Schwann cell-associated transcripts, and downregulated myelinating Schwann cell-associated transcripts. GO analyses showed upregulated collagens, cadherins, and metallopeptidases (i.e., extracellular matrix remodeling, cell adhesion and tissue development). All transcripts commonly involved in allograft rejection pathways were downregulated, whereas several transcripts commonly involved in immunosuppression or immune evasion were highly upregulated in PEG-fused PNAs compared to NC PNAs and Unoperated Control nerves, including CD24,

THBS1, THBS2 and CD276. Some of these transcripts are also involved in extracellular matrix remodeling or cell adhesion, further emphasizing the role these processes may have in PEG-mediated immunosuppression.

Modulation of T cell activation and allorejection responses

The rejection of allogeneic tissue involves a set of complex interactions among antigens, MHC molecules, adhesion molecules, cytokines, chemokines, and transcription factors. Inhibiting any of these interactions can produce immunosuppressive effects and prolonged survival of allografts. The activation of T cell effector responses against donor cells (T cell proliferation, cytokine production, apoptosis, etc.) require immunological synapse formation with a peptide/MHC and T cell receptor (TCR) complex in combination with cytokines and various well-studied costimulatory molecules such as CD28, CD80 (B7.1), CD86 (B7.2), CD40, and CD40LG. CD28 is expressed on T cells where it binds to CD80 or CD86 on donor or host antigen presenting cells to assist in promoting signaling cascades that control T cell proliferation, differentiation into effector types, and cytokine production (10). CD40LG, expressed on T cells, binds to CD40 on other host T cells or antigen presenting cells such as macrophages and B cells to stimulate their differentiation and activation of effector responses. The CD28 co-stimulation pathway can be inhibited by the homologous receptor CTLA4, which competes with CD28 for binding of CD80 or CD86 (56). Co-stimulatory blockades using CTLA4-immunoglobulin fusions or anti-CD40LG antibodies have shown to be modestly effective in preventing rejection-associated immune responses. Interaction between the ligand CD274 and the receptor PDCD1 on cytotoxic T cells blocks their activation—a common mechanism for tumors to evade the immune system.

We found that each of these co-stimulatory molecules and their ligands (including CTLA4, PDCD1 and CD274) are significantly downregulated in PEG-fused PNAs compared to NC PNAs, suggesting that they are unlikely to play an important role in T cell suppression of PEG-fused PNAs. CD276 is highly upregulated in PEG-fused PNAs and is involved in co-inhibition of the CD28 pathway. CD276 expression is inhibited by a microRNA, miR-29, that also inhibits extracellular matrix production and cell proliferation (49, 57). These data suggest a linkage between fibrogenesis and modulation of the immune response.

T cell proliferation, survival, and effector functions are largely controlled by cytokine stimulation, especially IL-2, IL-12, IFN-γ and IL-17 (10). Their associated signaling pathways are regulated via JAK/STAT signaling and transcription factors NFAT and NF-kB (both downregulated in PEG-fused PNAs), and/or RAR-related orphan receptor gamma T (RORγT). IL-2 is produced primarily in activated Th1 cells and functions as both an autocrine and a paracrine factor by stimulating rapid proliferation and differentiation of both CD8 and CD4 effector T cells (32). IL-12 is produced by antigen presenting cells such as macrophages and dendritic cells and acts as a powerful inducer of IFN-γ in Th1 and cytotoxic T cells (31). IFN-γ serves many functions in rejection, such as maintaining T cell survival, inducing MHC expression in nearby cells and inducing macrophages to produce pro-inflammatory cytokines and ROS (33). IL-17 is produced by Th17 cells and stimulates proinflammatory cytokine production, antigen presentation, and may suppress myelin production in Schwann cells (34). We observed that PEG-fused PNAs exhibit significant downregulation of each of these critical cytokines, as well as effector molecules FASL, PRF1, and GZMB that are commonly employed by cytotoxic T cells to kill donor cells.

The production of these cytokines in T cells can be inhibited via IL-10 and/or TGF-β1 stimulation from regulatory T cells (Tregs). Treg-mediated suppression of Th1 and Th2 responses is a common method of

immune evasion in both tolerated allografts as well as many types of cancer (35). However, we report that transcription of IL-10 and TGF-β1, as well as FOXP3, the transcription factor driving Treg differentiation, are all significantly downregulated in PEG-fused PNAs. These results suggest that inhibition of innate inflammatory processes that precede T cell recruitment, suppression of antigen presentation, and/or physical blockades of immune cell migration are responsible for PEG-fusion-mediated immunosuppression in PNAs.

When comparing PEG-fused PNAs and Unoperated Control nerves, we found that each of the factors described above are upregulated in PEG-fused PNAs. These results indicate that an adaptive immune response is still present within PEG-fused PNAs, although significantly less so than in NC PNAs.

Regulation of damage-recognition responses in innate immunity

An innate inflammatory response to surgical injury first must be initiated for other adaptive immune cells (T cells, etc.) and other innate immune cells to migrate to injured allograft tissue (8, 9). Following injury and during Wallerian degeneration, damaged and/or degenerating cells and axons within PNAs release damage-associated molecular patterns (DAMPs) such as HMGB1 and ATP. These substances are recognized via TLRs by resident innate immune cells (such as macrophages) or non-immune cells (such as Schwann cells). DAMP binding to these receptors triggers innate immune cells and activated Schwann cells to release an inflammatory milieu via signaling pathways such as NF-kB. This, in turn, recruits and potentiates adaptive immune cells to carry out a rejection response. In Schwann cells, these events coincide with differentiation from a myelinating state to a demyelinated state that facilitates myelin clearance and regeneration of axonal sprouts (3, 5).

We have found that many toll-like receptors, including TLR1, TLR4, and TLR9 were downregulated in PEG-fused PNAs compared to NC PNAs. Innate inflammatory responses were down regulated such as macrophage differentiation, including NFKB1 and downstream inflammatory cytokine IL1B, as well as NOS2, which contributes to oxidative damage (8). These results confirm and expand upon our previous immunohistochemistry-based assessment of reduced innate inflammatory responses in PEG-fused PNAs. IL1B and NOS2 are commonly produced by the classically activated M1 macrophage phenotype. Their reduction combined with increased expression of Arginase I and MRC1 in PEG-fused PNAs suggests a shift in macrophage polarization from a pro-inflammatory M1 state to an alternatively activated anti-inflammatory M2 state that contributes to wound healing. Numerous axons and Schwann cells in the PNA remain intact, functional, and nondegenerate following PEG-fusion repair. These results suggest that an effective response to tissue damage by resident Schwann cells or macrophages is impaired, possibly due to a significant prevention of tissue damage through PEG-fusion. Other studies have found that transplanted tissues treated with PEG via organ storage solution or intraluminal infusion had reduced inflammation and improved cell viability (58). Diminished ischemia reperfusion injury as a result of reduced mitochondrial swelling and ROS production, as well as restoration of membrane integrity in these tissues may also contribute to the amelioration of DAMP-mediated responses in PEG-fused PNAs. The upregulation of M1-associated inflammatory factors in PEG-fused PNAs compared to Unoperated Control nerves suggests that damage-recognition and innate immune responses in PEG-fused PNAs are attenuated rather than eliminated.

Our analyses of Schwann cell-associated transcripts revealed upregulation of factors that drive both the myelinating Schwann cell state (SOX10, MBP, CDH2) as well as the demyelinating state (JUN, SOX2, NGFR) within PEG-fused PNAs compared to NC PNAs. This elevation in common Schwann cell-associated transcripts in PEG-fused PNAs may underlie greater survival of Schwann cells in PEG-fused PNAs. In parallel, GO processes involved in both positive and negative regulation of tissue development and cell differentiation were enriched. Within cross-sections of PEG-fused PNAs sampled from 21-42d PO, regions of successfully PEG-fused axons with myelinating Schwann cells and unsuccessfully PEG-fused regions that have undergone Wallerian degeneration have been observed via electron microscopy (17). Compared to Unoperated Control nerves, the downregulation of myelinating Schwann cell-associated genes is likely attributed to these unsuccessfully PEG-fused regions. Generally, PNAs that have greater PEG-fusion success and greater functional recovery by 42d PO have a greater ratio of large-caliber myelinated axons to small-caliber demyelinated axons (17). A large population of myelinating Schwann cells and resident macrophages in successfully PEG-fused PNAs by 14d PO should not be associated with axons that have undergone Wallerian degeneration. Therefore, these Schwann cells and nearby resident macrophages would likely not activate an inflammatory signaling cascade due to a lack of DAMPs from their axons.

In the nervous system, CD24 is expressed in Schwann cells and developing neurons (47). CD24 inhibits dorsal root ganglion neurite outgrowth and adhesion via interaction with sialic acid binding lectin L1 on axonal membranes (59). High expression of CD24 in PEG-fused PNAs relative to Unoperated Control nerves may be related to the processes of neurite outgrowth following degeneration of unsuccessfully PEG-fused axons. However, CD24 could be more closely associated with myelinating or non-myelinating Schwann cells. The slight increase of CD24 expression in NC PNAs relative to Unoperated Control nerves suggests that CD24 is more closely associated with the demyelinated state. CD24, when bound to Siglec-10 on immune cells, can inhibit the immune response to many common cytoplasmic and nuclear DAMPs (47, 48). However, this effect seems to be at odds with the proinflammatory response to DAMPs typically associated with demyelinated Schwann cells following injury.

Factors controlling chemotaxis and extravasation into allograft tissue

Following the initial inflammatory response, immune cells must migrate via chemotaxis to extravasate through the endothelial lumen to reach the graft tissue (10). These processes are largely governed by chemokines such as CCL1/2/5 and CXCL9/10/11, as well as intercellular adhesion molecules such as selectins, ICAMs, and VCAMs that mediate cell rolling and diapedesis. After passing through the lumen, the extracellular matrix surrounding the entry site must be degraded by metallopeptidases such as MMP3 to grant full entry. We found that each major chemokine that attracts T cells and macrophages, as well as most adhesion molecules involved in extravasation, are downregulated in PEG-fused PNAs compared to NC PNAs. These results suggest that immune cells may not easily penetrate the inner region of a PEG-fused PNA.

Unexpectedly, a number of metallopeptidases (MMP3/11/23) were upregulated in PEG-fused PNAs. These molecules typically are expressed during injury and inflammation (60). These data suggest that metallopeptidase overexpression in PEG-fused PNAs plays an important role in extracellular matrix remodeling during resolution of injury and wound healing.

One of the most prominent findings of this study is the substantial upregulation of many extracellular matrix components in PEG-fused PNAs compared to NC PNAs and Unoperated Control nerves, including an extensive array of collagens and fibroblast growth factors. The extracellular matrix not only provides structural support to tissue components, but also participates in a wide variety of signaling events that regulate the behaviors of nearby cells. Collagens, laminins, and fibronectins make up the main components of peripheral nerve ECM (61). The epineurium and perineurium of peripheral nerves is composed mostly of fibrillar type I, II, and III collagens synthesized by fibroblasts, and the endoneurium containing the Schwann cell basement membrane consists of type IV and V collagens and laminins that assist in controlling myelination (62). Several other types of collagens, such as type XI, serve as networks that link additional fibrillar collagen strands or promote their polymerization (63).

Following traumatic nerve injury, fibroblasts proliferate and upregulate fibrillar collagen production to excessive amounts as part of scar formation (21, 61). Excessive collagen production can act as a mechanical barrier to axonal regeneration following injury and a dense collagen matrix also can physically block T cells from infiltrating certain types of solid tumors (64). T cells preferentially accumulate in areas of low collagen density and have greater difficulty migrating and contacting target cells in areas of high collagen density. A recent study has shown that dense collagen also inhibits the ability of T cells to proliferate, to produce cytotoxic molecules and to kill tumor cells (65).

We suggest that many myelinating Schwann cells in PEG-fused PNAs do not respond to injury stimuli, but fibroblasts do respond. Excessive collagen production by these fibroblasts might create an environment in which intact Schwann cell-axon units are surrounded by a dense collagen matrix. This would physically block T cells from accessing Schwann cells and fibroblasts, as well as inhibit their molecular activities. High expression of THBS1 and THBS2, which are integral to collagen formation processes and can have potent T cell suppression properties, might further bolster protection (51, 52). One might then assume that excessive collagen production in rejected PNAs not treated with PEG would also provide the same immunomodulatory effect. In contrast, we suggest that donor fibroblasts in untreated PNAs are also targets for rejection, thereby limiting collagen production. A combination of Schwann cell quiescence and other immunosuppressive properties conferred by PEG treatment may inhibit inflammatory signaling.

Antigen processing and presentation in PEG-fused PNAs

The coordination of antigen processing and presentation of MHC molecules in donor cells and host antigen presenting cells is carried out by a number of proteases, transport molecules, and binding proteins. Endogenous peptide fragments are generated in cytoplasmic proteasomes and are then transported into the endoplasmic reticulum via TAP1 and TAP2 proteins, where they are loaded onto MHC class I molecules (10). Exogenous peptide fragments enter the cell via endocytosis, where they are cleaved within lysosomes by proteases such as cathepsins D and L before being loaded onto MHC class II molecules. The expression of MHC class I and II subunits is controlled by the transcription factors NOD-like Receptor C5 (NLRC5) and Class II Major Histocompatibility Complex Transactivator (CIITA), respectively, and are upregulated by IFN-γ stimulation during injury and inflammation (66, 67).

Our transcriptomic analyses expand upon our previous IHC analyses showing that PEG-fused PNAs have significantly reduced MHC I and II protein expression compared to NC PNAs. We now report that the

transcription of a number of integral components of antigen processing and presentation are also significantly downregulated. This downregulation includes TAP1, TAP2, NLRC5, CIITA, and a wide variety of MHC subunits such as Beta-2-Microglobulin (B2M), RT1-DB1, RT1-CE3, and RT1-M3-1. These results suggest that the ability of donor cells to present antigen to host T cells is severely compromised, thereby decreasing their immunogenicity.

Cathepsins D and L are upregulated in PEG-fused PNAs (Additional File 4: Table S2). Aside from their assistance in antigen processing, these proteases perform a number of additional functions within tissues. These cathepsins are usually in cytoplasmic lysosomes, but can be secreted into the extracellular environment, where they cleave matrix components such as fibronectins, collagens, and laminins (68, 69). Procathepsin D has been shown to stimulate proliferation and motility in stromal fibroblasts (70). Overexpression of cathepsin D also has been associated with impaired antigen processing of T cell epitopes generated from myoglobin. Dendritic cells lacking cathepsin D demonstrate enhanced presentation of these epitopes (71). We suggest that increasing the concentration of cathepsin D in PEG-fused PNAs may lead to an increased number of cleavage sites on peptides, resulting in their destruction rather than their appropriate cleavage into presentable fragments.

Our results suggest that both PEG-fused PNAs and Unoperated Control nerves significantly upregulate Adenylyl Cyclase 8 (ADCY8) and Phosphodiesterase 1C (PDE1C) that catalyze cyclic AMP (cAMP) production and turnover. The myelinating state of Schwann cells is largely controlled by axonal contact through interactions between laminins on the Schwann cell basement membrane and the G-protein coupled receptor GPR126 (72). This interaction stimulates cAMP in Schwann cells that stimulates transcription of promyelinating genes, such as Early Growth Response 2 (EGR2) (73). cAMP also activates Protein Kinase A (PKA), which inhibits induction of MHCII by phosphorylating its central regulatory transcription factor, CIITA (74). Myelinating Schwann cells do not express MHCII but do express MHCI at low levels (75, 76). Demyelinated Schwann cells, on the other hand, do express high levels of MHCII and also upregulate expression of MHCI. PEG-fusion may affect the myelinating state of Schwann Cells via cAMP signaling. Taken together, these data suggest that a large number of Schwann cells in PEG-fused PNAs may demonstrate reduced immunogenicity solely due to their myelinating state.

Conclusions

This study is the first to examine altered cellular and molecular processes using a transcriptomic approach to assess PEG-fused PNAs that are immune-accepted even though they are neither immunosuppressed nor tissue-matched. This study is the first to identify a possible role for extracellular matrix remodeling in the immunosuppression of PEG-fused PNAs. Our data show that PEG-fused PNAs upregulate extracellular matrix remodeling, cell adhesion, and tissue development processes and Schwann cell-associated transcripts in both myelinating and demyelinated states, while significantly downregulating innate and adaptive immune responses necessary for allograft rejection. Maintenance of many myelinating Schwann cell-axon units in combination with extracellular matrix component production and reduced responses to cellular injury may contribute to an immunosuppressive environment within PEG-fused PNAs. The knowledge gained by these initial analyses of differential gene expression should generate new hypotheses for what molecular mechanisms underlie the immune acceptance of PEG-fused PNAs as a technique to repair ablation-type PNIs.

After ablation-type PNIs, recovery of lost behaviors in the clinical setting is often poor and has not significantly improved in decades despite advances in biomedical technologies (2, 7). Given that PEG-fusion of PNAs produces dramatic recovery within weeks of many lost behaviors and that these allografts are not rejected in the absence of tissue matching and/or immune suppression, PEG-fused PNAs have substantial potential to produce a paradigm shift in the clinical treatment of ablation-type PNIs.

Abbreviations

CAP: Compound action potential

CMAP: Compound muscle action potential

DAMP: Damage-associated molecular pattern

DAVID: Database for Annotation, Visualization, and Integrated Discovery

DEG: Differentially expressed gene

GO: Gene ontology

IHC: Immunohistochemistry

KEGG: Kyoto Encyclopedia of Genes and Genomes

MB: Methylene blue

MHC: Major histocompatibility complex

NC: Negative control

NGS: Next generation sequencing

PCA: Principle component analysis

PEG: Polyethylene glycol

PNA: Peripheral nerve allograft

PNI: Peripheral nerve injury

PO: Post-operatively

RNAseq: RNA sequencing

RT-qPCR: Quantitative reverse transcription PCR

TEM: Transmission electron microscopy

Unop: Unoperated Control nerve

Declarations

Ethics approval

All animal care, surgical procedures, and experimental procedures were approved by standards set forth by the Institutional Animal Care and Use Committee at the University of Texas at Austin and were conducted in accordance with the guidelines of the National Institutes of Health on the care and use of animals.

Consent for publication

Not applicable.

Availability of data and materials

The RNAseq datasets generated and/or analyzed during the current study are publicly available in the NCBI Gene Expression Omnibus (GEO) repository (accession #: GSE145504) (https://www.ncbi.nlm.nih.gov/geo/query/acc.cgi?acc=GSE145504). Primers for RT-qPCR were designed via the PrimerQuest tool by Integrated DNA Technologies (IDT) using complimentary mRNA transcript sequences derived from National Center for Biotechnology Information (NCBI) GenBank databases for *Rattus norvegicus* (www.ncbi.nlm.nih.gov/genbank; RRID:SCR_002760). All other data generated or analyzed during this study are included in this published article [and its supplementary information files].

Competing interests

Dr. Bittner has assigned all of his economic interests in a licensed PEG-fusion patent estate to a third party that affects in no way any data analyses or text in this manuscript.

Funding

This work was supported by grants from the Lone Star Paralysis Foundation and NIH grant R01 NS081063 to GDB and NIH Grant R01CA31534, Cancer Prevention Research Institute of Texas (CPRIT) Grants RP100612, RP120348; and the Marie Betzner Morrow Centennial Endowment to HOT.

Authors' contributions

All authors designed experiments. TAS performed surgeries, behavioral testing, electrophysiology, RNA extraction, RT-qPCR, and all bioinformatics analyses following initial generation of differential expression results. CLG performed surgeries, behavioral testing, and electrophysiology. All authors analyzed and interpreted data, wrote, and edited the paper. HOT and GDB supervised the project.

Acknowledgements

We thank Dr. Jianjun Shen and the Next Generation Sequencing Core staff at the MD Anderson Cancer Center (MDACC) Science Park in Smithville, TX for their excellent work and support.

References

1. Taylor CA, Braza D, Rice JB, Dillingham T. The incidence of peripheral nerve injury in extremity trauma. Am. J. Phys. Med. Rehabil. 2008;87(5): 381-385; doi: 10.1097/PHM.0b013e31815e6370. 2. Campbell WW. Evaluation and management of peripheral nerve injury. Clin Neurophysiol. 2008;119(9):1951-1965; doi: 10.1016/j.clinph.2008.03.018. 3. DeFrancesco-Lisowitz A, Lindborg JA, Niemi JP, Zigmond RE. The neuroimmunology of degeneration and regeneration in the peripheral nervous system. Neuroscience. 2015; 302:174-203; doi: 10.1016/j.neuroscience.2014.09.027. 4. Venereau E, Ceriotti C, Bianchi ME. DAMPs from cell death to new life. Front. Immunol. 2015;6:422; doi: 10.3389/fimmu.2015.00422. 5. Jessen KR, Mirsky R, Lloyd AC. Schwann cells: development and role in nerve repair. Cold Spring Harb. Perspect. Biol. 2015;7:a020487; doi: 10.1101/cshperspect.a020487. 6. Brushart TM. Nerve Repair. Oxford University Press; 2011. 7. Evans PJ, Midha R, Mackinnon SE. The peripheral nerve allograft: a comprehensive review of regeneration and neuroimmunology. Prog. Neurobiology. 1994;43:187-233, doi: 10.1016/0301-0082(94)90001-9. 8. Moreau A, Varey E, Anegon I, Cuturi MC. Effector mechanisms of rejection. Cold Spring Harb Perspect. Med. 2013;3:a015461; doi: 10.1101/cshperspect.a015461. 9. Land WG. Emerging role of innate immunity in organ transplantation Part I: evolution of innate immunity and oxidative allograft injury. Transplantation Reviews. 2012;26: 60-72; doi: 10.1016/j.trre.2011.05.001. 10. Murphy K, Weaver C. Janeway's Immunobiology. 9th ed. Garland Science; 2017. 11. Mika SE, Stepnowski P. Current methods of the analysis of immunosuppressive agents in clinical materials: A review. J. Pharm. Biomed. Anal. 2016;127:207–231; doi: 10.1016/j.jpba.2016.01.059. 12. Sachanandani NF, Pothula A, Tung TH. Nerve Gaps. Plast. Reconstr. Surg. 2014;133(2):313-319; doi: 10.1097/01.prs.0000436856.55398.0f. 13. Jiang H, Wynn C, Pan F, Ebbs A, Erickson LM, Kobayashi M. Tacrolimus and cyclosporine differ in their capacity to overcome ongoing allograft rejection as a result of their differential abilities to inhibit interleukin-10 production. Transplantation. 2002;73(11):1808-1817; doi: 10.1097/00007890-200206150-00019. 14. Mackinnon SE, Doolabh VB, Novak CB, Trulock EP. Clinical outcome following nerve allograft transplantation. Plast. Reconstr. Surg. 2001;107(6):1419-1429; doi: 10.1097/00006534-200105000-00016. 15. Bittner GD, Sengelaub DR, Trevino RC, Peduzzi JD, Mikesh M, Ghergherehchi CL, et al. The curious ability of PEG-fusion technologies to restore lost behaviors after nerve severance. J. Neurosci. Res. 2016;94:207-230; doi: 10.1002/jnr.23685. 16. Mikesh M, Ghergherehchi CL, Hastings RL, Ali A, Jagannath K, Sengelaub DR, et al. Polyethylene glycol solutions rapidly restore and maintain axonal continuity, neuromuscular structures, and behaviors lost after sciatic nerve transections in female rats. J. Neurosci. Res. 2018;96(7):1223-1242; doi: 10.1002/jnr.24225. 17. Mikesh M, Ghergherehchi CL, Rahesh S, Jagannath K, Ali A, Sengelaub DR, et al. Polyethylene glycol treated allografts not tissue matched nor immunosuppressed rapidly repair sciatic nerve gaps, maintain neuromuscular junctions, and restore voluntary behaviors in female rats. J. Neurosci. Res. 2018;96(7):1243-1264; doi: 10.1002/jnr.24227. 18. Bittner GD, Keating CP, Kane JR, Britt JM, Spaeth CS, Fan JD, et al. Rapid, effective, and long-lasting recovery produced by microsutures, methylene blue, and polyethylene glycol after completely cutting rat sciatic nerves. J Neurosci Res. 2012;90:967-980; doi: 10.1002/jnr.23023. 19. Smith TA, Ghergherehchi CL, Mikesh M, Tucker HO, Bittner GD. Polyethylene glycol-fusion repair of sciatic allografts in female rats achieve immunotolerance via attenuated innate and adaptive responses. J. Neurosci. Res. 2020 – In press. 20. Ansselin AD, Pollard JD. Immunopathological factors in peripheral nerve allograft rejection: quantification of lymphocyte invasion and major histocompatibility complex expression. J. Neurol. Sci. 1990;96:75-88; doi: 10.1016/0022-510x(90)90058-u. 21. Pollard JD, Fitzpatrick L. An Ultrastructural comparison of peripheral nerve allografts and autografts. Acta neuropath. 1973;23:152-165; doi: 10.1007/bf00685769. 22. Ghergherehchi CL, Mikesh M, Sengelaub DR, Jackson DM, Smith T, Nguyen J et al.

Polyethylene glycol (PEG) and other bioactive solutions with neurorraphy for rapid and dramatic repair of peripheral nerve lesions by PEG-fusion. J. Neurosci. Methods. 2019;314:1-12; doi: 10.1016/j.jneumeth.2018.12.015. 23. Love MI, Huber W, Anders S. Moderated estimation of fold change and dispersion for RNA-seq data with DESeq2. Genome Biol. 2014;15(12): 550; doi: 10.1186/s13059-014-0550-8. 24. Su G, Morris JH, Demchak B, Bader GD. Biological network exploration with Cytoscape 3. Curr. Protoc. Bioinformatics. 2014;47:13.1-24; doi: 10.1002/0471250953.bi0813s47. 25. Maere S, Heymans K, Kuiper M. BiNGO: a Cytoscape plugin to assess overrepresentation of gene ontology categories in biological networks. Bioinformatics. 2005; 21(16):3448-3449; doi: 10.1093/bioinformatics/bti551. 26. Kanehisa M, Furumichi M, Tanabe M, Sato Y, Morishima K. KEGG: new perspectives on genomes, pathways, diseases and drugs. Nucleic Acids Res. 2017;45(D1): D353–D361; doi: 10.1093/nar/gkw1092. 27. Mitchell AL, Attwood TK, Babbitt PC, Blum M, Bork P, Bridge A, et al. InterPro in 2019: improving coverage, classification and access to protein sequence annotations. Nucleic Acids Res. 2019;47(D1):D351-D360; doi: 10.1093/nar/gky1100. 28. Huang DW, Sherman BT, Tan Q, Collins JR, Alvord WG, Roayaei J, et al. The DAVID Gene Functional Classification Tool: a novel biological module-centric algorithm to functionally analyze large gene lists. Genome Biol. 2007;8(9):R183; doi: 10.1186/gb-2007-8-9-r183. 29. Szklarczyk D, Gable AL, Lyon D, Junge A, Wyder S, Huerta-Cepas J, et al. STRING v11: protein-protein association networks with increased coverage, supporting functional discovery in genome-wide experimental datasets. Nucleic Acids Res. 2019;Jan; 47:D607-613; doi: 10.1093/nar/gky1131. 30. Livak KJ, Schmittgen TD. Analysis of relative gene expression data using real-time quantitative PCR and the 2-ΔΔCT method. Methods. 2001;25:402-408; doi: 10.1006/meth.2001.1262. 31. Wojno EDT, Hunter CA, Stumhofer JS. The immunobiology of the interleukin-12 family: room for discovery. Immunity. 2019;50(4):P851-870; doi: 10.1016/j.immuni.2019.03.011. 32. Arenas-Ramirez N, Woytschak J, Boyman O. Interleukin-2: Biology, Design and Application. Trends in Immunology. 2015;36(12):763-777; doi: 10.1016/j.it.2015.10.003. 33. Schroder K, Hertzog PJ, Ravasi T, Hume DA. Interferon-γ: an overview of signals, mechanisms and functions. J. Leukocyte Biol. 2004;75:163-189; doi: 10.1189/jlb.0603252. 34. Stettner M, Lohmann B, Wolffram K, Weinberger JP, Dehmel T, Hartung HP, et al. Interleukin-17 impedes Schwann cell-mediated myelination. J. Neuroinflammation. 2014;11:63; doi: 10.1186/1742-2094-11-63. 35. Schmidt A, Oberle N, Krammer PH. Molecular mechanisms of Treg-mediated T cell suppression. Front. Immunol. 2012;3(51): 1-20; doi: 10.3389/fimmu.2012.00051. 36. Wan YY. GATA3: a master of many trades in immune regulation. Trends in Immunology. 2014;35(6):233-242; doi: 10.1016/j.it.2014.04.002. 37. Murray PJ. Macrophage polarization. Annu. Rev. Physiol. 2017;79:541-566; doi: 10.1146/annurev-physiol-022516-034339. 38. Chistiakov DA, Killingsworth MC, Myasoedova VA, Orekhov AN, Bobryshev YC. CD68/macrosialin: not just a histochemical marker. Laboratory Investigation. 2017;97:4-13; doi: 10.1038/labinvest.2016.116. 39. Pittelli M, Cavone L, Lapucci A, Oteri C, Felici R, Niccolai E, et al. Nicotinamide phosphoribosyltransferase (NAMPT) activity is essential for survival of resting lymphocytes. Immunol. Cell Biol. 2014;92(2):191-199; doi: 10.1038/icb.2013.85. 40. Yanagisawa H, Schluterman MK, Brekken RA. Fibulin-5, an integrin-binding matricellular protein: its function in development and disease. J. Cell Commun. Signal. 2009; 3(3-4):337-347; doi: 10.1007/s12079-009-0065-3. 41. Maruyama M, Hattori A, Goto Y, Ueda M, Maeda M, Fujiwara H, et al. Laeverin/aminopeptidase Q, a novel bestatin-sensitive leucine aminopeptidase belonging to the M1 family of aminopeptidases. J. Biol. Chem. 2007;282(28):20088-20096; doi: 10.1074/jbc.M702650200. 42. Feinberg K, Eshed-Eisenbach Y, Frechter S, Amor V, Salomon D, Sabanay H, et al. A Glial Signal Consisting of Gliomedin and NrCAM Clusters Axonal Na+ Channels during the Formation of Nodes of Ranvier. Neuron. 2010;65(4):490-502; doi: 10.1016/j.neuron.2010.02.004. 43. Caputo S, Bellone M. Osteopontin and the immune system:

another brick in the wall. Cell. Mol. Immunol. 2018;15(4):405-407; doi: 10.1038/cmi.2017.94. 44. Engeland K. Cell cycle arrest through indirect transcriptional repression by p53: I have a DREAM. Cell Death Different. 2018;25:114-132; doi: 10.1038/cdd.2017.172. 45. Hayashi S, Inoue Y, Kiyonari H, Abe T, Misaki K, Moriguchi H, et al. Protocadherin-17 mediates collective axon extension by recruiting actin regulator complexes to interaxonal contacts. Dev. Cell. 2014;30(6):673-687; doi: 10.1016/j.devcel.2014.07.015. 46. Takada Y, Ye X, Simon S. The integrins. Genome Biology. 2007;8(5):215; doi: 10.1186/gb-2007-8-5-215. 47. Gilliam DT, Menon V, Bretz NP, Pruszak J. The CD24 surface antigen in neural development and disease. Neurobiol. Dis. 2017;99:133-144; doi: 10.1016/j.nbd.2016.12.011. 48. Barkal AA, Brewer RE, Markovic M, Kowarsky M, Barkal SA, Zaro BW, et al. CD24 signalling through macrophage Siglec-10 is a new target for cancer immunotherapy. Nature. 2019;572(7769):392-396; doi: 10.1038/s41586-019-1456-0. 49. Calabro NE, Barrett A, Chamorro-Jorganes A, Tam S, Kristofik NJ, Xing H, et al. Thrombospondin-2 regulates extracellular matrix production, LOX levels, and cross-linking via downregulation of miR-29. Matrix Biol. 2019;82:71-85; doi: 10.1016/j.matbio.2019.03.002. 50. Rosini S, Pugh N, Bonna AM, Hulmes DJS, Farndale RW, Adams JC. Thrombospondin-1 promotes matrix homeostasis by interacting with collagen and lysyl oxidase precursors and collagen cross-linking sites. Science Signaling. 2018;11(532):eaar2566; doi: 10.1126/scisignal.aar2566. 51. Miller MW, Kaur S, Ivins-O'Keefe K, Roberts DD. Thrombospondin-1 is a CD47-dependent endogenous inhibitor of hydrogen sulfide signaling in T cell activation. Matrix Biology. 2013;32(6):316-324; doi: 10.1016/j.matbio.2013.02.009. 52. Lamy L, Foussat A, Brown EJ, Bornstein P, Ticchioni M, Bernard A. Interactions between CD47 and Thrombospondin reduce inflammation. J. Immunol. 2007;178:5930-5939; doi: 10.4049/jimmunol.178.9.5930. 53. Castellanos JR, Purvis IJ, Labak CM, Guda MR, Tsung AJ, Velpula KK, et al. B7-H3 role in the immune landscape of cancer. Am. J. Clin. Exp. Immunol. 2017;6(4):66-75. 54. Ueno T, Yeung MY, McGrath M, Yang S, Zaman N, Snawder B, et al. Intact B7-H3 signaling promotes allograft prolongation through preferential suppression of Th1 effector responses. Eur. J. Immunol. 2012;42(9):2343-2353; doi: 10.1002/eji.201242501. 55. Hüser L, Sachindra S, Granados K, Federico A, Larribère L, Novak D, et al. SOX2-mediated upregulation of CD24 promotes adaptive resistance toward targeted therapy in melanoma. Int. J. Cancer. 2018;143(12):3131-3142; doi: 10.1002/ijc.31609. 56. Seidel JA, Otsuka A, Kabashima K. Anti-PD-1 and Anti-CTLA-4 Therapies in Cancer: Mechanisms of Action, Efficacy, and Limitations. Front. Oncol. 2018;8(86) 1-14; doi: 10.3389/fonc.2018.00086. 57. Xu H, Cheung IY, Guo HF, Cheung NK. MicroRNA miR-29 modulates expression of immunoinhibitory molecule B7-H3: potential implications for immune based therapy of human solid tumors. Cancer Res. 2009;69(15):6275-6281; doi: 10.1158/0008-5472.CAN-08-4517. 58. Thuillier R, Giraud S, Favreau F, Goijon JM, Desurmont T, Eugene M, et al. Improving long-term outcome in allograft transplantation: role of ionic composition and polyethylene glycol. Transplantation. 2011;91:605-614; doi: 10.1097/TP.0b013e3182090fa3. 59. Kleene R, Yang H, Kutsche M, Schachner M. The Neural Recognition Molecule L1 Is a Sialic Acid-binding Lectin for CD24, Which Induces Promotion and Inhibition of Neurite Outgrowth. J. Biol. Chem. 2001;276:21656-21663; doi: 10.1074/jbc.M101790200. 60. Parks WC, Wilson CL, Lopez-Boado YS. Matrix metalloproteinases as modulators of inflammation and innate immunity. Nature Rev. Immunol. 2004;4:617-629; doi: 10.1038/nri1418. 61. Gonzalez-Perez F, Udina E, Navarro X. Extracellular matrix components in peripheral nerve regeneration. Int. Rev. Neurobiol. 2013;108:257-275; doi: 10.1016/B978-0-12-410499-0.00010-1. 62. Koopmans G, Hasse B, Sinis N. Chapter 19: The role of collagen in peripheral nerve repair. Int. Rev. Neurobiol. 2009;87:363-379; doi: 10.1016/S0074-7742(09)87019-0. 63. Vaughan-Thomas A, Young RD, Phillips AC, Victor CD. Characterization of Type XI Collagen-Glycosaminoglycan Interactions. J. Biol. Chem. 2001;276(7): 5303–5309; doi: 10.1074/jbc.M008764200. 64.

Salmon H, Franciszkiewicz K, Damotte D, Dieu-Nosjean MC, Validire P, Trautmann A, et al. Matrix architecture defines the preferential localization and migration of T cells into the stroma of human lung tumors. J. Clin. Invest. 2012;122(3):899-910; doi: 10.1172/JCI45817. 65. Kuczek DE, Larsen AMH, Thorseth ML, Carretta M, Kalvisa A, Siersbæk MS, et al. Collagen density regulates the activity of tumor-infiltrating T cells. J. Immunother. Cancer. 7(1):68; doi: 10.1186/s40425-019-0556-6. 66. Ludigs K, Seguin-Estevez Q, Lemeille S, Ferrero I, Rota G, Chelbi S, et al. NLRC5 Exclusively Transactivates MHC Class I and Related Genes through a Distinctive SXY Module. PLoS Genetics. 2015;11(3):e1005088; doi: 10.1371/journal.pgen.1005088. 67. Masternak K, Muhlethaler-Mottet A, Villard J, Zufferey M, Steimle V, Reith W. CIITA is a transcriptional coactivator that is recruited to MHC class II promoters by multiple synergistic interactions with an enhanceosome complex. Genes and Dev. 2000;14:1156-1166. 68. Benes P, Vetvicka V, Fusek M. Cathepsin D - many functions of one aspartic protease. Crit. Rev. Oncol. Hematol. 2008;68(1):12-28; doi: 10.1016/j.critrevonc.2008.02.008. 69. Turk V, Stoka V, Vasiljeva O, Renko M, Sun T, Turk B, et al. Cysteine cathepsins: From structure, function and regulation to new frontiers. Biochim. Biophys. Acta. 2012;1824(1):68-88; doi: 10.1016/j.bbapap.2011.10.002. 70. Beaujouin M, Prébois C, Derocq D, Laurent-Matha V, Masson O, Pattingre S, et al. Pro-cathepsin D interacts with the extracellular domain of the β chain of LRP1 and promotes LRP1-dependent fibroblast outgrowth. J. Cell Sci. 2010;123(Pt 19):3336-3346; doi: 10.1242/jcs.070938. 71. Moss CX, Villadangos JA, Watts C. Destructive potential of the aspartyl protease cathepsin D in MHC class II-restricted antigen processing. Eur. J. Immunol. 2005;35(12):3442-3451; doi: 10.1002/eji.200535320. 72. Petersen SC, Luo R, Liebscher I, Giera S, Jeong SJ, Mogha A, et al. The adhesion GPCR GPR126 has distinct, domain-dependent functions in Schwann cell development mediated by interaction with laminin-211. Neuron. 2015;85(4):755-769; doi: 10.1016/j.neuron.2014.12.057. 73. Bacallao K, Monje PV. Requirement of cAMP signaling for Schwann cell differentiation restricts the onset of myelination. PLoS One. 2015;10(2):e0116948; doi: 10.1371/journal.pone.0116948. 74. Li G, Harton JA, Zhu X, Ting JPY. Downregulation of CIITA Function by Protein Kinase A (PKA)-Mediated Phosphorylation: Mechanism of Prostaglandin E, Cyclic AMP, and PKA Inhibition of Class II Major Histocompatibility Complex Expression in Monocytic Lines. Mol. Cell Biol. 2001;21(14):4626-4635; doi: 10.1128/MCB.21.14.4626-4635.2001. 75. Bombeiro AL, Thomé R, Nunes SLO, Moreira BM, Verinaud L, de Oliveira ALR. MHC-I and PirB Upregulation in the Central and Peripheral Nervous System following Sciatic Nerve Injury. PLoS One. 2016;11(10):e0165185; doi: 10.1371/journal.pone.0161463. 76. Lisak RP, Bealmear B, Benjamins JA. Schwann cell differentiation inhibits interferon-gamma induction of expression of major histocompatibility complex class II and intercellular adhesion molecule-1. J. Neuroimmunol. 2016;295:93-99; doi: 10.1016/j.jneuroim.2016.03.013.

Additional File Legends

Additional file 1: Fig. S1 (FigS1_Exp_Design.pdf). Outline of the experimental design of the study. PEG-fused sciatic nerve allografts (“PEG”, *n*=3 animals), negative control sciatic nerve allografts (“NC”, *n*=3 animals) from outbred Sprague Dawley rats were excised and sampled 14d post-operatively. Both treatment groups were compared to Unoperated Control sciatic nerves (“Unop”, *n*=2 animals). Total RNA was extracted from each sample via homogenization with TRIzol (Ambion) and a RNeasy Mini kit (Qiagen). Libraries were prepared using a TruSeq Stranded mRNA kit (Illumina), which were then sequenced on a HiSeq 3000 unit (Illumina). Analysis of read results was carried out sequentially by FastQC, Tophat2, HTSeq-count, and

DESeq2 software. Subsequent analyses were performed via DAVID and the STRING application for Cytoscape software. Validation of candidate genes was performed via RT-qPCR, using the same treatment groups.

Additional file 2: Table S1 (RNAseq_Reads_Table.xlsx). Read mapping and alignment results for all samples used for RNAseq. The ID of each animal is indicated underneath the sample name in parentheses.

Additional file 3: Fig. S2 (FigS2_Count_Analyses.pdf). Distribution and correlation of normalized read counts between samples. (A) Violin plots showing the distribution of all $\log_2$ normalized read counts for each gene transcript in each sample. The median is indicated by a solid horizontal line, and the upper quartile is indicated by a dashed horizontal line. The plots show that the majority of genes in each sample share similar expression profiles and are not differentially expressed. **(B)** Principle component analysis (PCA) allowing clustering of samples based on variation in expression profiles of all protein coding genes. Samples with similar expression profiles cluster together more closely. **(C)** Sample-to-sample correlation matrix comparing the gene expression profiles of all coding genes between all individual samples, using normalized read counts. White indicates a Pearson correlation coefficient of <0.6 (lower correlation); black indicates a coefficient of 1 (high correlation).

Additional file 4: Table S2 (Differential_Expression_Results.xlsx). Excel tables showing **(Tab 1)** all normalized read counts for all samples and associated gene transcripts, **(Tab 2)** PEG vs NC differential expression results, **(Tab 3)** PEG vs Unop differential expression results, and **(Tab 4)** NC vs Unop differential expression results.

Additional file 5: Table S3 (DEG_Heatmap_Clusters.xlsx). Excel tables showing **(Tab 1)** Z-scores of all 2,180 transcripts extracted from the DEG heatmap displayed in Fig. 2A, which heatmap cluster each transcript is associated with (Cluster 1, 2, 3, or 4), and the PEG vs NC differential expression results for each transcript, **(Tab 2)** all transcripts associated with Cluster 1 and their PEG vs NC differential expression results, **(Tab 3)** all transcripts associated with Cluster 2 and their PEG vs NC differential expression results, **(Tab 4)** all transcripts associated with Cluster 3 and their PEG vs NC differential expression results, and **(Tab 5)** all transcripts associated with Cluster 4 and their PEG vs NC differential expression results.

Additional file 6: Table S4 (GO_KEGG_InterPro_Clusters.xlsx). Excel tables showing **(Tabs 1-3)** GO, KEGG and InterPro results for Cluster 1 (high expression in PEG), **(Tabs 4-6)** GO, KEGG and InterPro results for Cluster 2 (high expression in PEG and Unop), **(Tabs 7-9)** GO, KEGG and InterPro results for Cluster 3 (high expression in Unop), and **(Tabs 10-12)** GO, KEGG and InterPro results for Cluster 4 (high expression in NC).

Additional file 7: Fig. S3 (FigS3_BiNGO_Diagram_Clusters.pdf). Enlarged versions of the BiNGO cluster diagrams displayed in Figs. 3A-D, in which each cluster can be zoomed-in on with clarity to view all associated GO annotations and their interrelations. **(Page 1)** Cluster 1 (enriched in PEG), **(Page 2)** Cluster 2 (enriched in PEG and Unop), **(Page 3)** Cluster 3 (enriched in Unop), **(Page 4)** Cluster 4 (enriched in NC).

Figures

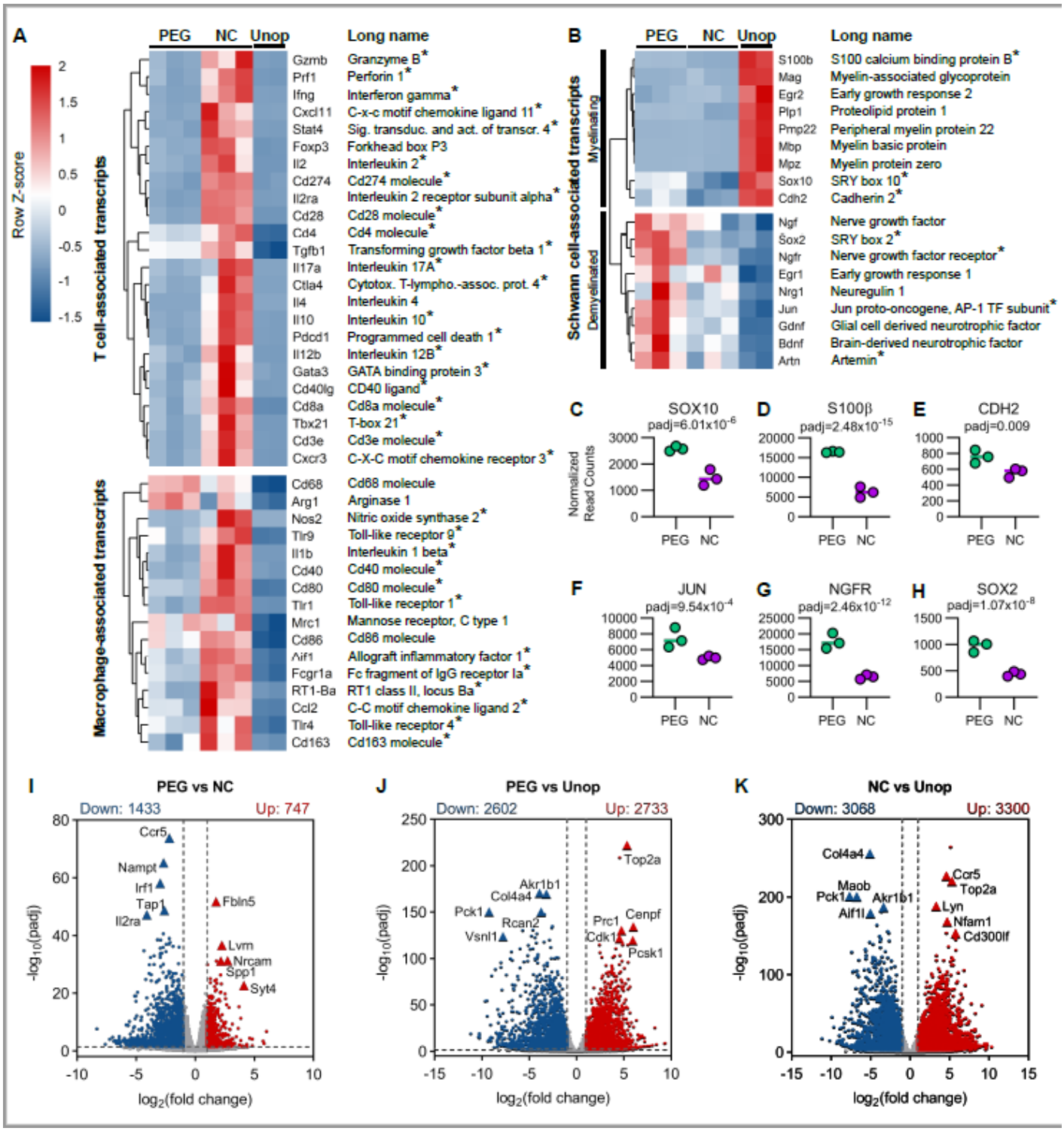

Figure 1

Cell-type associated transcripts and differentially expressed genes (DEGs) among PEG-fused allografts, NC allografts, and Unoperated Control nerves. (A) Heatmap showing relative expression of T cell-associated transcripts and macrophage-associated transcripts between all samples using normalized read counts. Each column is a sample, and each row is a gene. Transcripts are hierarchically clustered based on expression patterns across rows. Red = high expression; blue = low expression. Transcripts with statistically significant differences in expression (padj<0.05) when compared between PEG and NC groups are marked with an

asterisk. (B) Heatmap showing relative expression of Schwann cell-associated transcripts. (C-H) Normalized read counts of Schwann cell-associated transcripts that are significantly upregulated (PEG vs NC, padj<0.05). Horizonal bars indicate the mean. (I-K) Volcano plots showing all DEGs between (I) PEG vs NC, (J) PEG vs Unop, and (K) NC vs Unop. Thresholds for log2 fold changes >1 or <-1 and padj<0.05 were used to identify greatly upregulated (red) or downregulated (blue) DEGs for subsequent analyses. The number of up- or downregulated DEGs in each comparison is shown above each plot. Each point represents a single gene transcript. Triangles indicate notable DEGs that have very low adjusted p-values (padj).

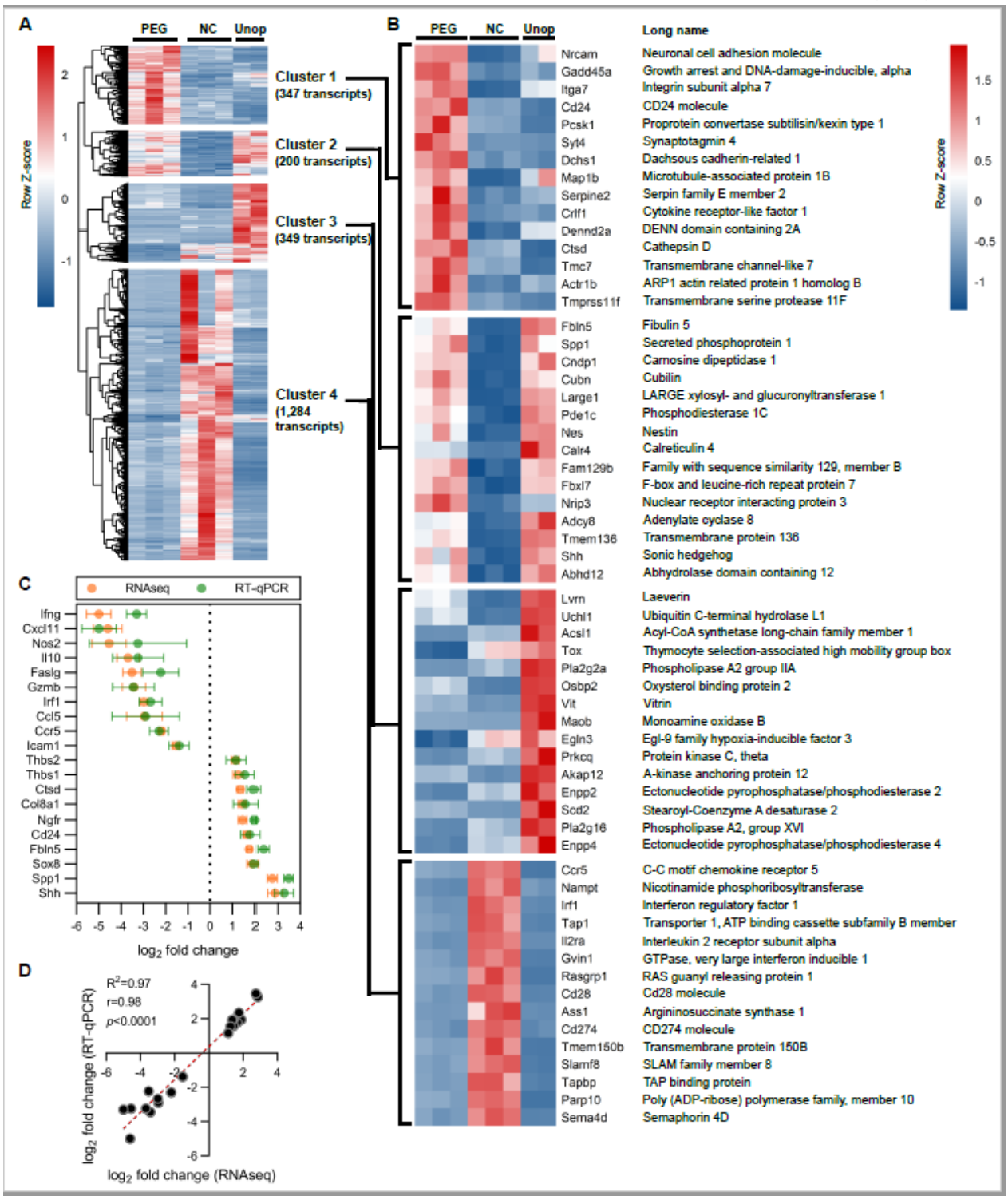

Figure 2

Division of DEGs into clusters based on expression patterns between treatment groups; validation of RNAseq results. (A) Heatmap showing relative expression of transcripts based on normalized read counts for all DEGs with log2 fold changes >1 or <-1 and padj<0.05 among PEG and NC groups (2,180 DEGs total). Red = high expression; blue=low expression. The heatmap is split into 4 distinct clusters of expression patterns among treatment groups, based on k-means clustering: Cluster 1 (highest expression in PEG), Cluster 2 (high expression in both PEG and Unop), Cluster 3 (highest expression in Unop), and Cluster 4 (highest expression in NC). (B) Heatmaps showing the top 15 DEGs in each cluster, ranked by padj (PEG vs NC comparison). (C) Comparison of log2 fold changes between RNAseq and RT-qPCR for 10 upregulated and 10 downregulated transcripts of interest (comparing PEG vs NC) that are represented in Clusters 1, 2, or 4. Data represents the mean ± SEM (n=3 animals per treatment group). (D) Correlation of RNAseq and RT-qPCR results from Fig. 2C, using linear regression and Pearson Correlation analyses. Each point indicates a specific transcript.

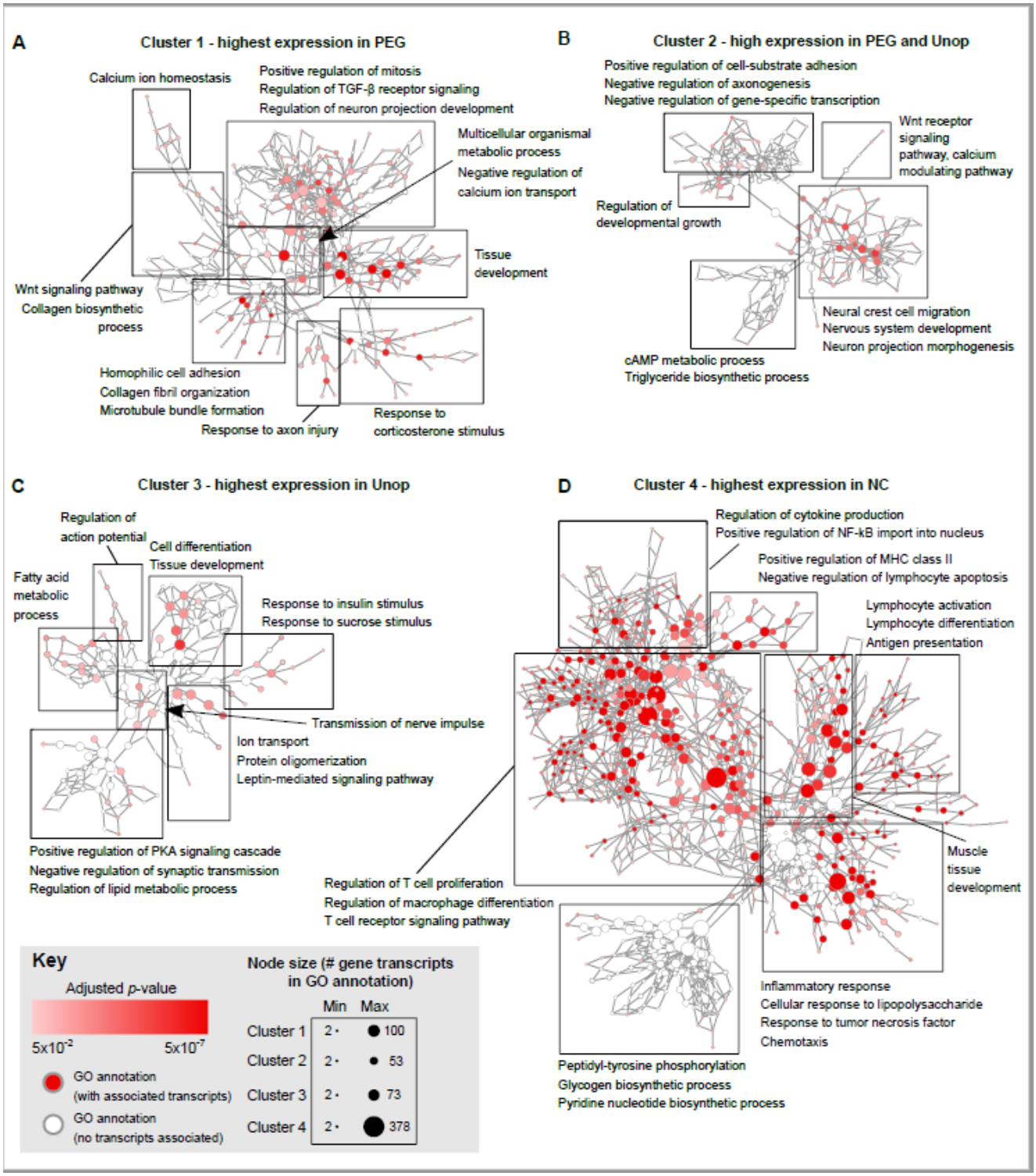

Figure 3

Visualization of overrepresented biological processes in Clusters 1-4 using BiNGO for gene ontology (GO) analysis. Each node in the networks for (A) Cluster 1, (B) Cluster 2, (C) Cluster 3, and (D) Cluster 4 represents a single GO annotation for an overrepresented biological process. The size of the node corresponds to the number of transcripts associated with the GO annotation, while the color shade of the node indicates the padj of each GO annotation (Hypergeometric test; Benjamini & Hochberg False Discovery Rate correction; threshold padj<0.05). Deeper color = lower padj. Blank nodes do not contain transcripts associated with Clusters 1-4.

Networks are organized hierarchically from broader “parent” terms containing large numbers of transcripts (e.g. “cellular process”) to more specific “child” terms containing fewer numbers of transcripts (e.g. “regulation of T cell proliferation”). Families of similar GO annotations are grouped into boxes; representative GO annotations contained within are indicated next to each box. A zoomed-in view of each network and GO annotation can be viewed in (Additional File 7: Fig. S3). Note that GO biological processes are not the same as pathways, but rather a grouping of molecular activities contributing to a single event.

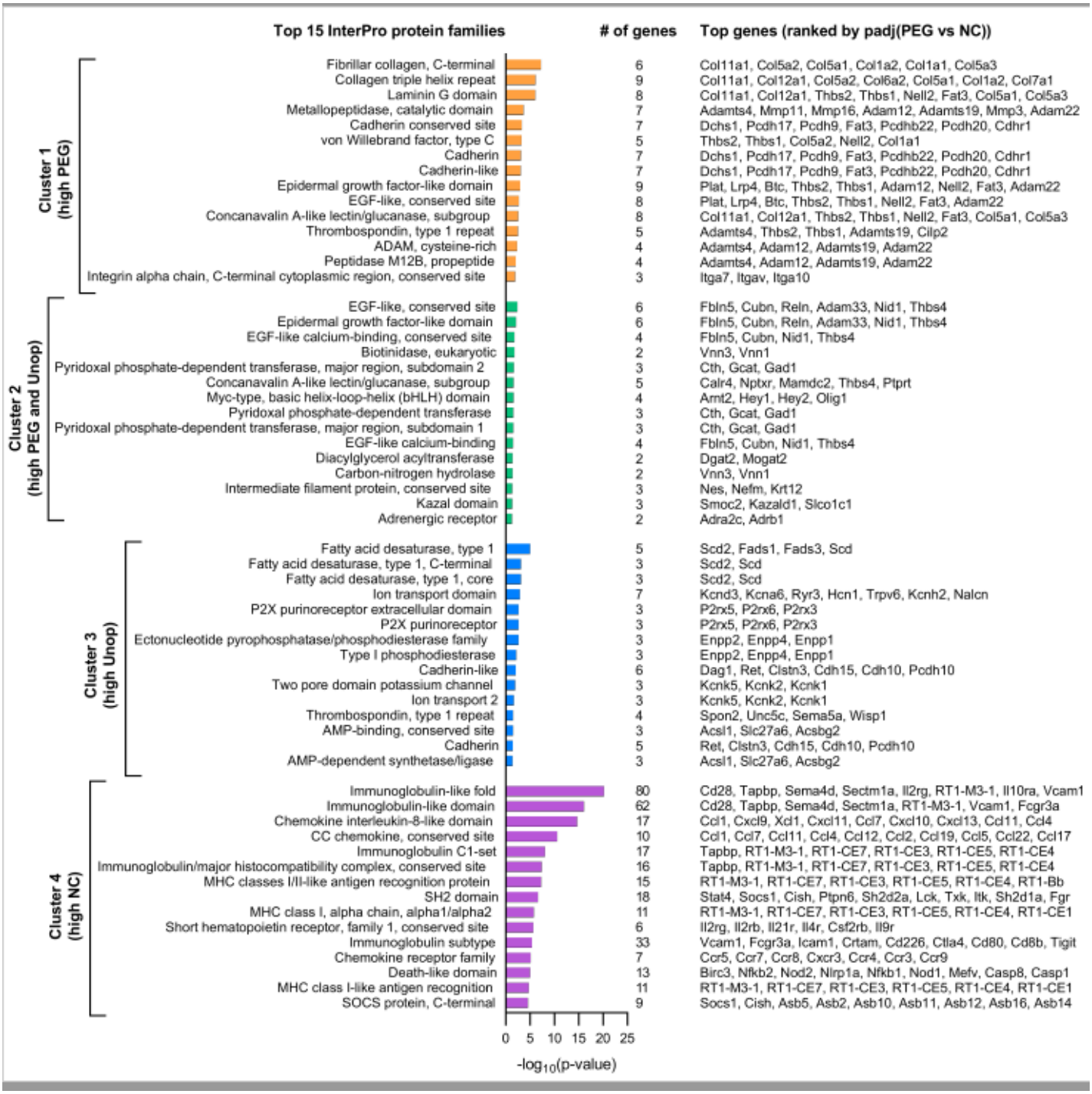

Figure 4

Top 15 overrepresented InterPro protein families in Clusters 1-4. InterPro terms in each cluster are ranked by p-value (Fisher Exact test). The number of transcripts associated with each term as well as the top associated

transcripts (ranked by padj (PEG vs NC comparison) are indicated. Note that a single transcript may be associated with more than one term.

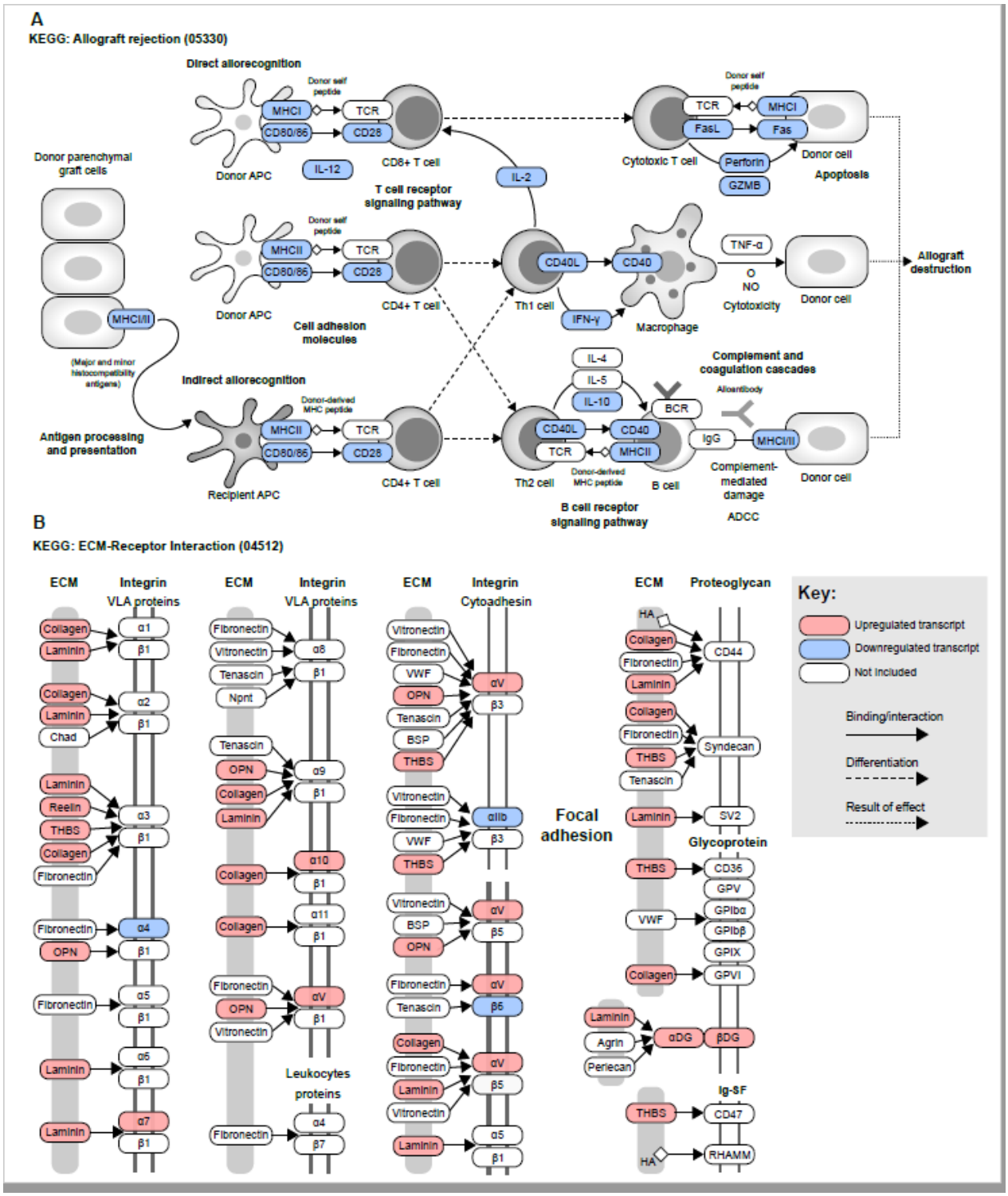

Figure 5

Mapping of RNAseq data (PEG vs NC) to top KEGG pathways from Clusters 1 and 4. (A) Allograft rejection pathway (2nd most highly enriched for downregulated transcripts in the PEG vs NC comparison) showing key molecules and processes involved in allograft rejection (ordered left to right in the diagram). Upregulated transcripts (pink tiles), downregulated transcripts (blue tiles), and transcripts that are part of the pathway, but

not included in our list of DEGs (white tiles) are shown. Solid arrows represent protein interactions, while dashed arrows pointing to or from T cells represent T cell differentiation into effector phenotypes. Dotted arrows point to the result of an effect. (B) ECM-receptor interaction pathway (most highly enriched for upregulated transcripts in the PEG vs NC comparison) showing binding interactions between extracellular matrix proteins and either integrins, proteoglycans, glycoproteins, or immunoglobulin superfamily (Ig-SF) members. These diagrams have been stylistically modified from the original KEGG diagrams for display purposes.

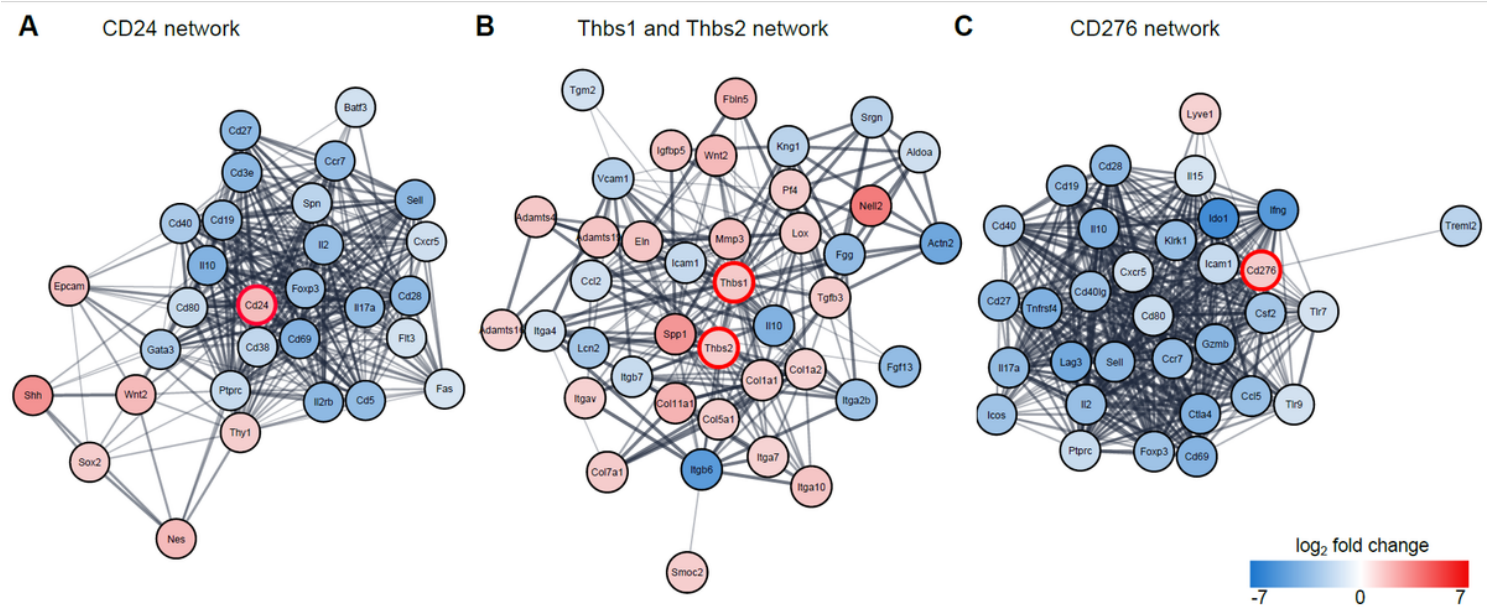

Figure 6

STRING protein-protein interaction networks of potentially immunosuppressive transcripts CD24, THBS1, THBS2, and CD276. (A-C) STRING protein-protein interaction networks of upregulated (red) and downregulated (blue) DEGs directly associated with (A) CD24, (B) THBS1 and THBS2, and (C) CD276. The list of transcripts used to create these networks was derived from all transcripts associated with Clusters 1, 2, and 4. Each node indicates a specific protein, shaded according to its log2 fold change value (PEG vs NC comparison). Pink = upregulated, blue = downregulated. Distances between nodes indicates greater or lesser association between proteins, while the thickness of the lines between nodes indicates the confidence score of the interaction (thicker = greater confidence, thinner = lesser confidence). The positions of CD24, THBS1, THBS2, and CD276 in each network are indicated by red borders.

Supplementary Files

This is a list of supplementary files associated with this preprint. Click to download.

- RNAseqReadsTable.xlsx
- FigS2CountAnalyses.pdf
- DifferentialExpressionResults.xlsx
- GOKEGGInterProClusters.xlsx

- FigS3BiNGODiagramClusters.pdf
- DEGHeatmapClusters.xlsx
- FigS1ExpDesign.pdf